Cell Chemical Biology

Subtype-selective prenylated isoflavonoids disrupt regulatory drivers of MYCN-amplified cancers

Graphical abstract

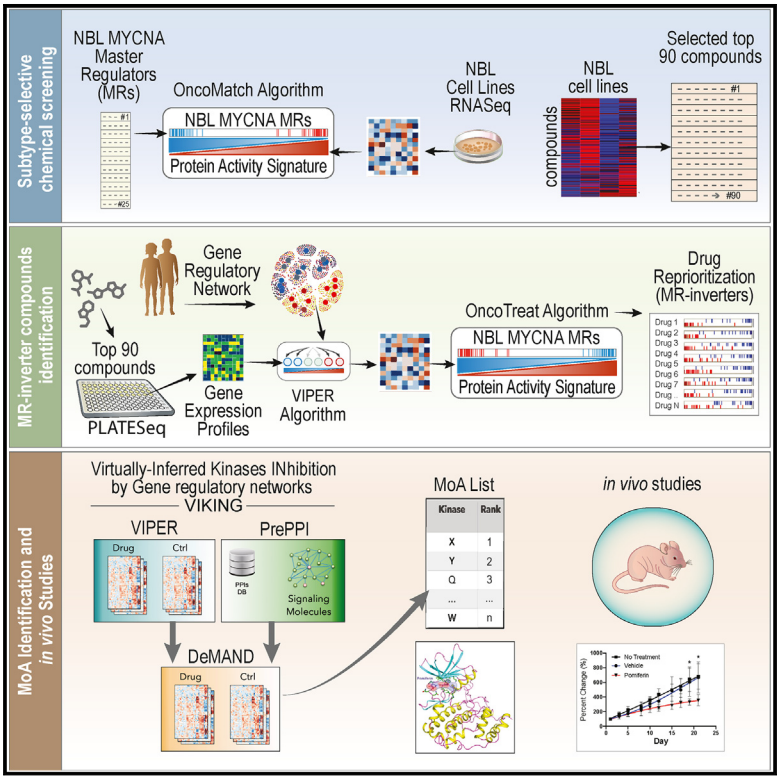

Highlights

- OncoTreat prioritized subtype-selective compounds that disrupt a regulatory module
- Top hits included prenylated isoflavonoid molecules that suppress MYCN protein
- Pomiferin suppressed MYCN *in vivo*, slowing growth of SK-N-Be2 NBL xenografts
- VIKING algorithm identified putative targets, including casein kinase2 (CK2)

Authors

Michael E. Stokes, Alessandro Vasciaveo, Jonnell Candice Small, ..., Presha Rajbhandari, Andrea Califano, Brent R. Stockwell

Correspondence

ac2248@cumc.columbia.edu (A.C.), bstockwell@columbia.edu (B.R.S.)

In brief

Stokes and Vasciaveo et al. evaluated selective agents targeting MYCN-amplified neuroblastoma cells using PLATE-Seq and regulatory network analysis. This revealed prenylated isoflavonoids that suppress a tumor checkpoint module, causing MYCN depletion and cell death. This paper highlights a multifaceted approach that enables screening for agents targeting networked drivers of disease.

Stokes et al., 2024, Cell Chemical Biology *31*, 1–15
April 18, 2024
https://doi.org/10.1016/j.chembiol.2023.11.007

CellPress

Cell Chemical Biology

CellPress

Resource

Subtype-selective prenylated isoflavonoids disrupt regulatory drivers of MYCN-amplified cancers

Michael E. Stokes,[1,7] Alessandro Vasciaveo,[2,7] Jonnell Candice Small,[1] Arie Zask,[1] Eduard Reznik,[1] Nailah Smith,[1] Qian Wang,[1] Jacob Daniels,[3] Farhad Forouhar,[4] Presha Rajbhandari,[1] Andrea Califano,[2,*] and Brent R. Stockwell[1,5,6,8,*]

[1]Department of Biological Sciences, Columbia University, New York City, NY 10027, USA
[2]Department of Systems Biology, Columbia University Medical Center, New York City, NY 10032, USA
[3]Department of Pharmacology, Columbia University Medical Center, New York City, NY 10032, USA
[4]Proteomics and Macromolecular Crystallography Shared Resource (PMCSR), Columbia University Medical Center, New York City, NY 10032, USA
[5]Department of Chemistry, Columbia University, New York City, NY 10027, USA
[6]Department of Pathology and Cell Biology and Herbert Irving Comprehensive Cancer Center, Columbia University Irving Medical Center, New York, NY 10032, USA
[7]These authors contributed equally
[8]Lead contact
*Correspondence: ac2248@cumc.columbia.edu (A.C.), bstockwell@columbia.edu (B.R.S.)
https://doi.org/10.1016/j.chembiol.2023.11.007

SUMMARY

Transcription factors have proven difficult to target with small molecules because they lack pockets necessary for potent binding. Disruption of protein expression can suppress targets and enable therapeutic intervention. To this end, we developed a drug discovery workflow that incorporates cell-line-selective screening and high-throughput expression profiling followed by regulatory network analysis to identify compounds that suppress regulatory drivers of disease. Applying this approach to neuroblastoma (NBL), we screened bioactive molecules in cell lines representing its MYC-dependent (MYCNA) and mesenchymal (MES) subtypes to identify selective compounds, followed by PLATESeq profiling of treated cells. This revealed compounds that disrupt a sub-network of MYCNA-specific regulatory proteins, resulting in MYCN degradation *in vivo*. The top hit was isopomiferin, a prenylated isoflavonoid that inhibited casein kinase 2 (CK2) in cells. Isopomiferin and its structural analogs inhibited MYC and MYCN in NBL and lung cancer cells, highlighting the general MYC-inhibiting potential of this unique scaffold.

INTRODUCTION

Neuroblastoma (NBL) is the most common extracranial solid tumor affecting children, responsible for ~15% of all pediatric cancer deaths each year.[1] NBL derives from the neural crest, an embryonic structure that gives rise to the sympathetic nervous system.[2] Tumors driven by focal amplification of the *MYCN* locus (MYCNA subtype)—occurring in ~20% of NBL patients—are associated with the most aggressive phenotype and poor prognosis.[3,4] Tumor stratification based on clinical, pathological, and genetic factors places patients into risk categories, with high risk NBL carrying 40–50% chance of survival.[1,5] Since there are no effective targeted therapies for the aggressive MYCNA subtype, this represents a substantial unmet medical need.

MYCN is considered an "undruggable" protein, due to lack of potential binding pockets on its surface amenable to small molecule docking. As MYCN abundance is determined by relative rates of synthesis and degradation, one strategy to target this protein is by modulating the upstream regulators of these processes. For example, disruption of the MYCN/AURK protein-protein interaction (PPI) by alisertib increases MYCN turnover by enabling access to a phosphodegradation site on MYCN.[6,7] Despite toxicity associated with AURKA inhibition in pediatric patients, this approach demonstrated that indirect MYCN targeting by small molecules is a viable strategy to inhibit activity in cells and tumors.

MYCNA-subtype homeostasis is regulated by a complex autoregulatory system that was elucidated by network-based analysis of primary tumor gene expression profiles.[8] This study revealed a tightly interacting ten-protein core set—or tumor checkpoint module (TCM)—driven by an aberrant MYCN-TEAD4 autoregulatory loop.[8] Genetic disruption of this module, via TEAD4 silencing, suppressed MYCN activity and abrogated tumor viability *in vitro* and *in vivo*, suggesting that targeting the TCM with small molecule inhibitors may be an effective strategy for the treatment of MYCNA-subtype tumors.[9] Here, we used this MYCNA-subtype-specific-TCM, comprising a 10-master-regulator-(MR)-proteins

Please cite this article in press as: Stokes et al., Subtype-selective prenylated isoflavonoids disrupt regulatory drivers of MYCN-amplified cancers, Cell Chemical Biology (2023), https://doi.org/10.1016/j.chembiol.2023.11.007

module, as a multiplexed phenotypic reporter assay to prioritize subtype-selective lethal molecules.

As TCM collapse abrogates MYCN activity and induces tumor demise *in vivo*, we leveraged the OncoTreat methodology[10] to identify compounds capable of inverting the activity of TCM MR proteins, identified as mechanistic determinants of MYCNA tumors. The approach relies on gene expression profiles of cells following perturbation with a panel of candidate drugs in 96-well format, produced by the PLATESeq technology.[11,12] OncoTreat assesses TCM inactivation by measuring the activity of its proteins in drug vs. vehicle-treated cells, using the VIPER algorithm—an extensively validated, network-based algorithm that, akin to a multiplexed gene reporter assay, measures protein activity based on the expression of their tissue-specific transcriptional targets.[13,14]

The top-ranked molecule emerging from this screen was a prenylated isoflavonoid, called isopomiferin, that collapsed the TCM and suppressed both MYCN and TEAD4 in MYCN-amplified NBL cells. Integrative analysis of isopomiferin-treated cells identified kinases as targets of isopomiferin and structurally related isoflavonoid molecules, including casein kinase 2 (CK2), which is a pleiotropic kinase that regulates a variety of cellular processes, including cellular proliferation.[15,16] We characterize the mechanism of this unique class of inhibitors that disrupt the MYCNA-TEAD4-centric TCM, leading to its inactivation and subsequent cell death. The methodology is generalizable and can be expanded across cancer types to identify selective compounds that suppress the regulatory architecture driving the disease-related cellular phenotype and to elucidate their mechanism of action.

RESULTS

A chemical screen identifies MYCNA-selective inhibitors

We hypothesized that a phenotypic screen for compounds with enhanced potency in MYCNA cell lines would identify subtype-selective molecules and enrich for compounds that disrupt the MYCNA TCM. To facilitate the screen, expression profiles from a comprehensive panel of NBL cell lines were evaluated using the OncoMatch algorithm to identify those that best recapitulate both the regulatory network and the aberrant activity of the MR protein identified from MYCNA primary tumor analysis.[8] Specifically, OncoMatch assesses the conservation of the top 25 most activated and 25 most inactivated MRs between each individual patient and the cell line model.[17] The analysis revealed SK-N-Be2 and IMR-32 as the MYCNA cell lines most closely recapitulating the regulatory network and MR profile observed in primary tumors. Two cell lines most representative of the mesenchymal NBL subtype (MES), SK-N-AS and NLF, were also included to control for subtype specificity of the compounds.

To identify subtype-selective inhibitors, we systematically screened >5,000 compounds from three chemical libraries chosen for their enrichment of bioactive molecules, diversity in chemical structure, and for inclusion of compounds with known mechanisms of action. Compounds were initially tested at a single concentration and time-point (20 μM for 72 h) to eliminate those with no *in vitro* activity in NBL cell lines. Lethal compounds were re-screened across a five-point dilution series ranging from 20 μM to ~250 nM, to determine IC_{50} values in each of the four cell lines. By ranking compounds based on average IC_{50} values for each of the two subtypes, MYCNA or MES-selective compounds were identified (Figure 1).[18]

PLATESeq analysis identifies compounds that disrupt the MYCNA TCM

The top 90 compounds with the highest relative MYCNA vs. MES specific selectivity were then used to generate PLATESeq expression profiles at 24 h following treatment of SK-N-Be2 cell lines with each compound at its IC_{20} concentration[11] (Figure 2A). PLATESeq relies on barcoding transcripts isolated from treated cells grown in 96-well plates, which are then pooled and sequenced, thus yielding 96 drug-specific gene expression profiles per plate. We then generated differential protein activity profiles by comparing the gene expression profile of compound vs. vehicle control (DMSO)-treated cells using the VIPER algorithm and assessed their ability to invert TCM MR activity using the OncoTreat algorithm. The latter is characterized by very high reproducibility, leading to its CLIA certification (Clinical Laboratory Improvement Amendments of 1988) in both New York and California. OncoTreat assesses a compound's ability to revert the aberrant activity of patient-derived MR proteins (i.e., MR-inverters), by performing a protein set enrichment analysis (PSEA) of patient-derived MRs in proteins that are most differentially activated following compound perturbation.[10,17] Statistically significant negative normalized enrichment scores (NESs) indicate strong activity reversal, driven by inhibition or activation of MR proteins by MR-inverter compound. Figure 2B shows a list of 90 compounds ranked by their inferred efficacy using this approach, along with the gene expression and protein activity profiles of the 10-MR protein module responsible for NBL MYCNA subtype. While there is no clear pattern of transcriptional repression among top inhibitors, using protein activity as a readout demonstrates that top MR-inverters effectively suppress the activity of virtually all proteins within the 10-MR module, including its core MYCN-TEAD4 positive feedback loop.

Across all TCGA (The Cancer Genome Atlas) tumor cohorts, an average of ≤50 master regulators were shown to integrate the effect of 90% of the tumor mutations, on a patient-by-patient basis.[19] We therefore used TCMs defined as the top 50 candidate MRs of the MYCNA subtype—i.e., 25 most activated and 25 most inactivated—to compute the activity reversion score. This score enabled us to prioritize MR-inverter compounds based on the ability to collapse the MYCNA TCM, including the core set of ten transcriptional regulators (TEAD4, PRDM8, ZNF219, E2F3, MYBL2, HMGB2, TAF1D, HNRNPAB, MYCN, and TFAP4) that were experimentally validated as mechanistic drivers of the aggressive MYCNA tumor subtype.[8] Of all 90 compounds tested using this methodology, isopomiferin had the strongest TCM reversal effect, suppressing the activity of virtually all ten aberrantly activated MR proteins comprising the MYCNA TCM (Figure 2B). Compound activity on master regulators is effectively recapitulated by gene set enrichment analysis (GSEA) plots, enabling visualization of MR differential activity following chemical perturbation. In these plots, transcriptional regulators are ranked based on inferred protein activity by VIPER algorithm, including the aberrantly activated (red) and suppressed (blue) master regulators of the MYCNA subtype.

Please cite this article in press as: Stokes et al., Subtype-selective prenylated isoflavonoids disrupt regulatory drivers of MYCN-amplified cancers, Cell Chemical Biology (2023), https://doi.org/10.1016/j.chembiol.2023.11.007

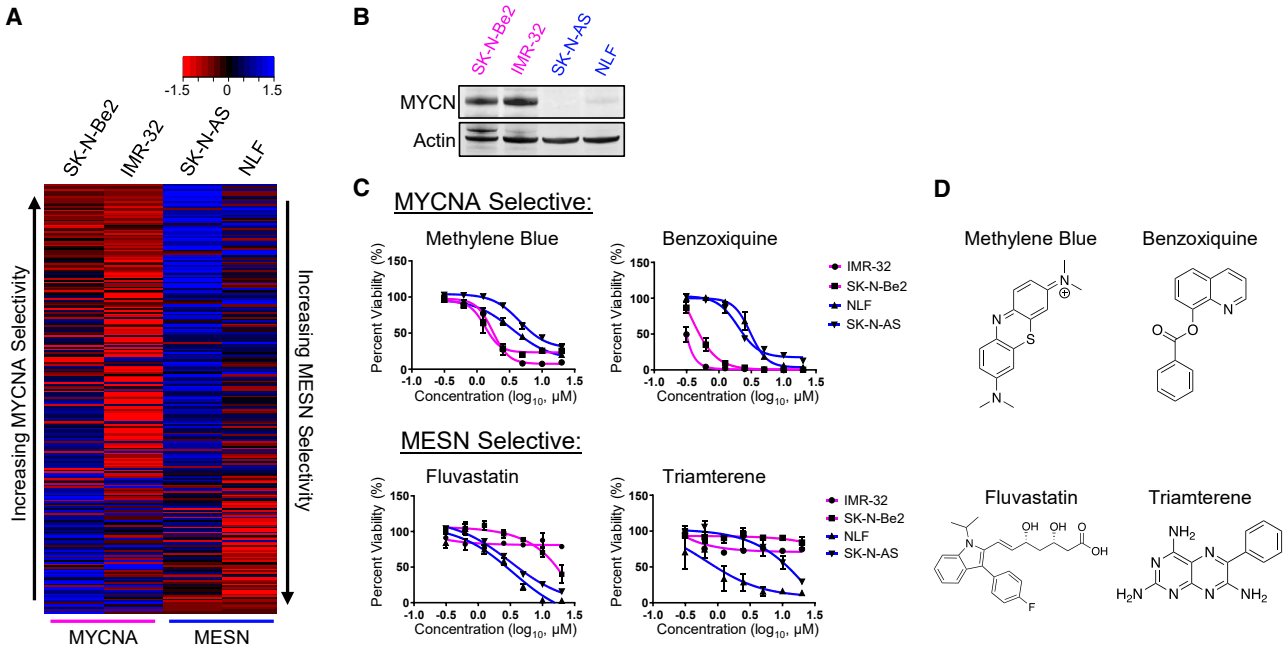

Figure 1. Chemical screen identifies subtype-selective compounds

(A) Heatmap of z-scores from row-normalized IC_{50} values. Compounds ranked on ratio of average IC_{50} of MYCNA cells over MESN cell line models.

(B) Western blot of MYCN protein expression in MYCNA and MESN cell lines.

(C) Dose-response curves from four NBL cell lines treated for 48 h. Data represent the mean from three replicate experiments, and error bars represent standard deviation across experiments (mean ± S.D.).

(D) Chemical structures of four subtype-selective compounds.

As shown, TCM-suppressing compounds inhibited activated master regulators and restored the activity of the inactivated ones (Figure 2C). Importantly, VIPER predicted that TCM-collapsing compounds suppress the activity of MYCN, while compounds that did not revert the signature would have negligible effect on MYCN activity.

The MYCNA TCM acts in coordinated fashion to establish and maintain the transcriptional state of the MYCNA subtype.[8] Genetic interrogation of these core regulatory proteins suggested that their activity is established by a positive feedback loop between MYCN and TEAD4, determined by both transcriptional and post-translational interactions, which is essential for cell viability.[8] We reasoned that compounds capable of disrupting the TCM would inhibit MYCN protein activity in MYCNA cell lines. To test this hypothesis, MYCN abundance was evaluated following treatment with the top five TCM-collapsing compounds (isopomiferin, homidium bromide, methyl gambogate methyl ether, podophyllotoxin, and NSC255109), compared to three negative control compounds that were not predicted to affect MYCN (Figure S1A). As potency differed between compounds, each molecule was tested at its IC_{20} concentration following 24 h of treatment, as well as at a 3-fold dilution. Consistent with VIPER results predicting MYCN suppression, the top-ranked compounds dramatically reduced MYCN protein abundance, while compounds that did not disrupt the TCM (negative controls) had no effect on MYCN abundance (Figure 2D).

Top TCM-reverting compounds were prioritized for follow up study based on reversion score, development opportunity, and novelty. Methyl gambogate methyl ether and podophyllotoxin were both potent inhibitors of cell viability and MYCN expression, decreasing protein abundance at 600 nM (Figure 2D). However, these compounds were deprioritized on account of development challenges and possible tolerability issues. Podophyllotoxin is an antimitotic agent that that is a chemical precursor to the cytotoxic chemotherapeutics etoposide and teniposide.[20] Gambonic acid and derivatives have broad apoptotic effects across cancer cell models at IC_{50} values consistent with our observations, but these natural products are challenged by poor solubility and pleiotropic cellular effects.[21] Although isopomiferin was less potent as an inducer of cell death, it scored highest of 96 molecules tested for TCM inversion and depleted MYCN in SK-N-Be2 cells at 5 μM. Little is known about isopomiferin's mechanism of action, which presented an opportunity to uncover novel facets of MYCN biology, especially in the context of the MYCNA subtype. As such, an investigation into the mechanisms through which isopomiferin disrupts the MYCNA TCM was undertaken.

We next sought to investigate biological pathways affected by isopomiferin by performing enrichment analysis on a set of 50 Cancer Hallmark pathways, comprising genes involved in cancer-specific bioprocesses and curated by the Broad Institute.[22] Additional PLATESeq profiles were generated from SK-N-Be2 cells at 6 h and 24 h following isopomiferin perturbation at 3.3 μM and 10 μM. We then analyzed the VIPER-inferred protein activity profiles of isopomiferin vs. DMSO-treated cells to study the compound's mechanism of action. Ten Cancer Hallmark gene sets were significantly enriched in differentially active proteins, across both time points and concentrations. Consistent

Please cite this article in press as: Stokes et al., Subtype-selective prenylated isoflavonoids disrupt regulatory drivers of MYCN-amplified cancers, Cell Chemical Biology (2023), https://doi.org/10.1016/j.chembiol.2023.11.007

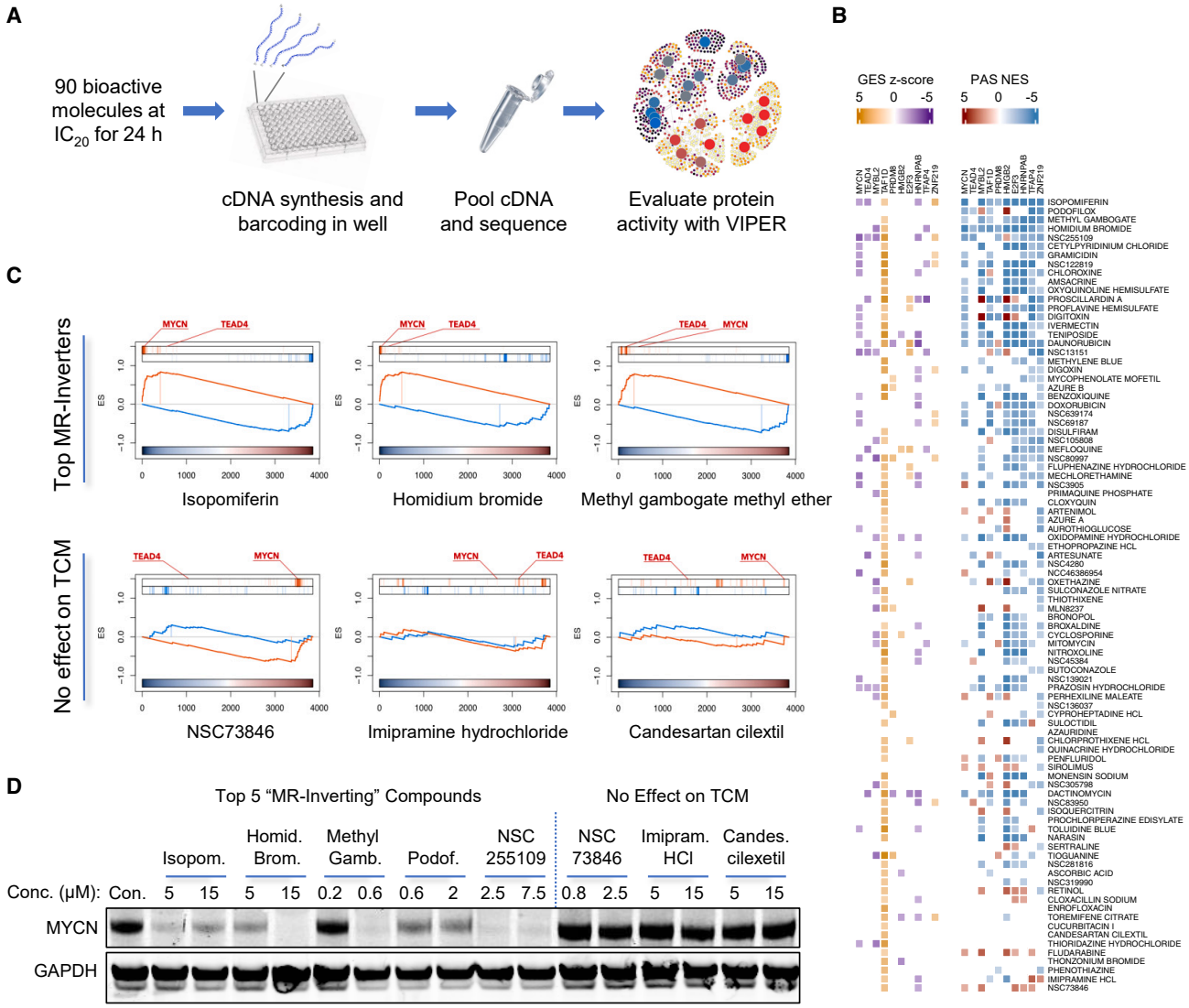

Figure 2. OncoTreat identifies lethal compounds that revert the MYCNA tumor checkpoint module (TCM)

(A) Schematic of PLATE-Seq workflow.

(B) Evaluating the effect of 90 compounds on the MYCNA TCM revealed hit molecules predicted to collapse the TCM and suppress MYCN activity. Showing gene expression z-scores on the left, and VIPER-inferred normalized enrichment scores (NES) on the right. (GES: Gene Expression Signature, PAS: Protein Activity Signature).

(C) VIPER GSEA plots of regulatory proteins ranked from low-to-high activity along x axis. Highlighted are 25 master regulators (MRs) that are upregulated (red) or suppressed (blue) in MYCNA tumors. Compounds that revert the signature suppress aberrantly activated proteins, including MYCN and TEAD4.

(D) Western blot of MYCN protein abundance in SK-N-Be2 cells treated with TCM-reverting compounds for 24 h (isopomiferin, homidium bromide, methyl gambogate methyl ether, podofilox, and NSC255109). Three non-reverting compounds included for comparison (NSC73846, imipramine hydrochloride, and candesartan cilexetil).

with the effect of isopomiferin on MYCN abundance and cell viability, gene sets associated with MYC activity (“MYC Targets”), and cell-cycle regulation (“E2F Targets” and “G2M Checkpoint”) were effectively suppressed by isopomiferin, in time- and dose-dependent manner (Figure 3A).

Isopomiferin induced dose-dependent decrease in MYCN abundance in SK-N-Be2 cells, which was validated across three other MYCNA cell models (Figures 3B and S1B). Isopomiferin subsequently triggers apoptosis, as indicated by cleaved caspase 3 and PARP cleavage (Figure 3G). At the protein level, MYCN is regulated by its relative synthesis and degradation rates.[23] As such, compounds affecting MYCN turnover will affect its overall abundance. Consistent with this, treatment with proteasome inhibitor MG132 abrogated isopomiferin’s ability to ablate MYCN, suggesting that an active proteasome is essential for the compound’s activity and that the compound works by affecting MYCN turnover (Figure 3C). We then looked at a network of MYCN-interacting proteins, and their first interacting neighbors, for the top 10 compounds as recovered from the PPI database (PrePPI). All top compounds suppressed MYCN

Please cite this article in press as: Stokes et al., Subtype-selective prenylated isoflavonoids disrupt regulatory drivers of MYCN-amplified cancers, Cell Chemical Biology (2023), https://doi.org/10.1016/j.chembiol.2023.11.007

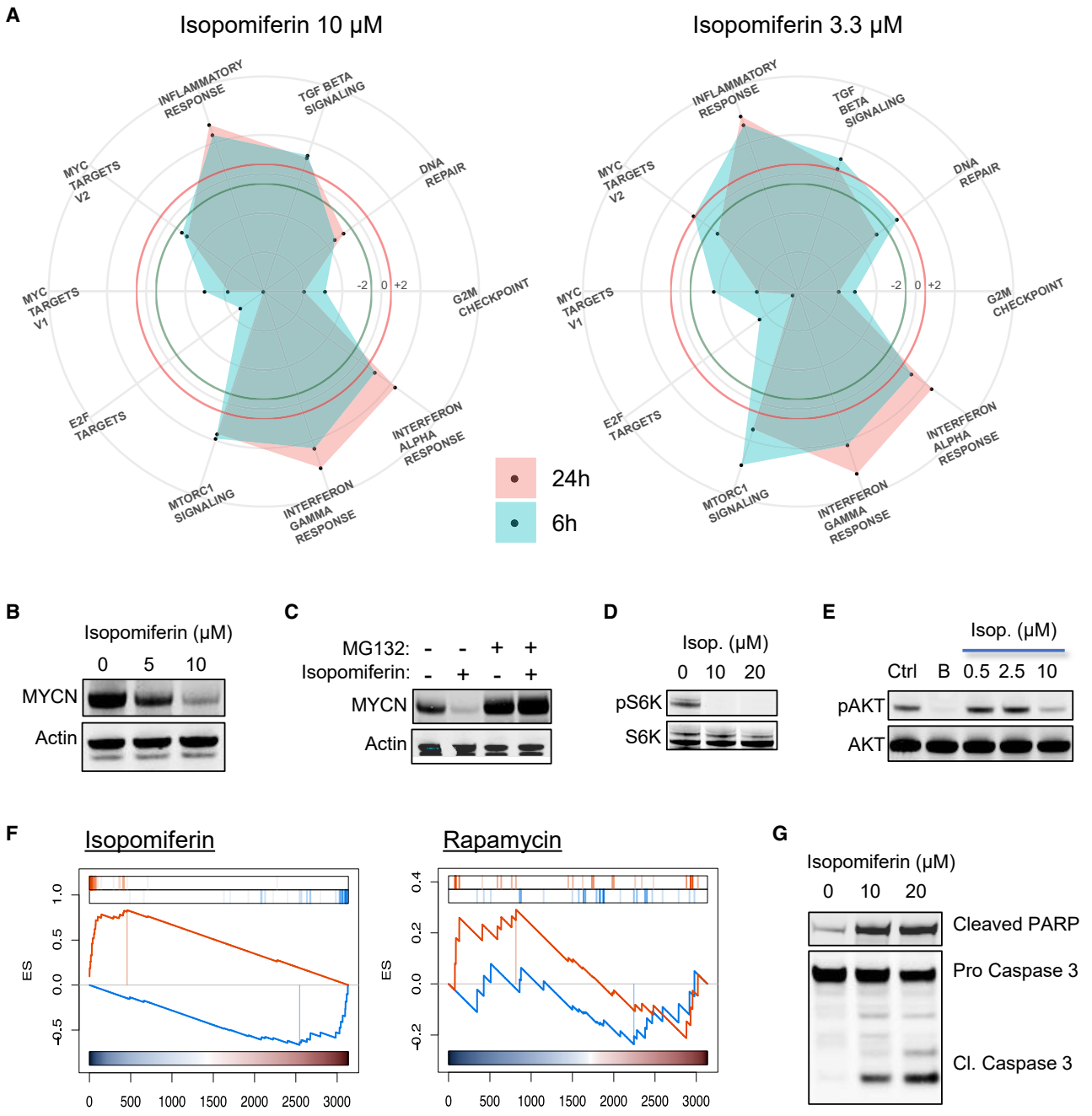

Figure 3. Isopomiferin induces degradation of MYCN

(A) Radar plots of pathways enrichment analysis using the hallmarks of cancer MSigDB gene set. The colored lines indicate statistical significance at $p < 0.05$; gene sets outside of the red line are enriched for activity, whereas gene sets inside the green are suppressed in protein activity.

(B) MYCN abundance in SK-N-Be2 cells treated with isopomiferin for 24 h, at indicated concentrations.

(C) Western blot analysis of MYCN abundance in SK-N-Be2 cells treated with 5 μM MG132 and 15 μM isopomiferin for 6 h.

(D) Western blot analysis of $P70^{S6K}$ phosphorylation levels following treatment with isopomiferin for 24 h. Total $P70^{S6K}$ used as a loading control.

(E) Measurement of AKT phosphorylation (Ser473) levels following treatment with isopomiferin for 24 h. Treatment with 250 nM BEZ-235 (B) used as a positive control. Total AKT used as loading control.

(F) VIPER GSEA plots of 10 μM isopomiferin or 1 μM rapamycin for 24 h.

(G) Western blot analysis of cleaved Caspase3 and cleaved PARP. SK-N-Be2 cells treated at indicated concentration of isopomiferin for 48 h.

protein (Figure S1C, negative VIPER scores in blue), albeit some showed a trend of protein activation for MYC or MAX (positive VIPER scores in red).

Previous studies have suggested potential mechanisms through which prenylated isoflavonoids inhibit cell proliferation. One study tested the effect of pomiferin triacetate on mTOR

Please cite this article in press as: Stokes et al., Subtype-selective prenylated isoflavonoids disrupt regulatory drivers of MYCN-amplified cancers, Cell Chemical Biology (2023), https://doi.org/10.1016/j.chembiol.2023.11.007

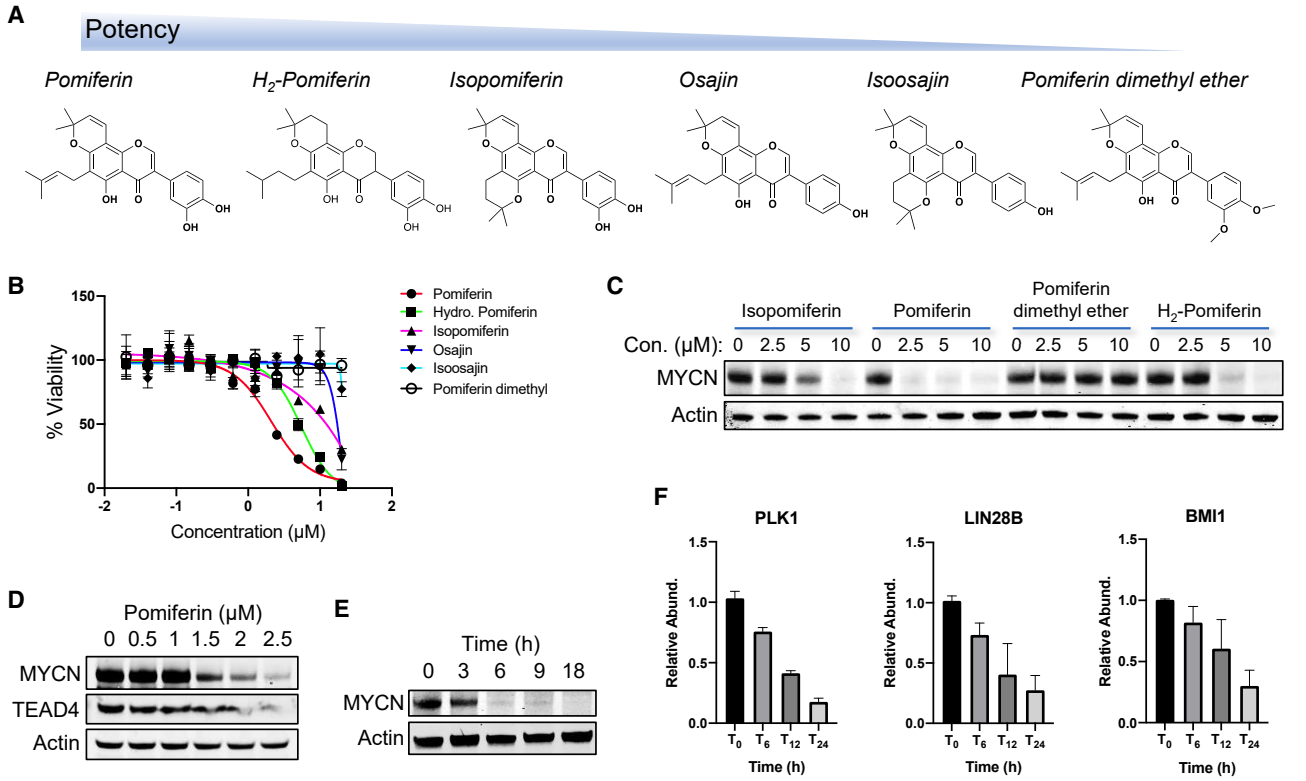

Figure 4. Structural analogs reveal a potent MYCN inhibitor and preliminary SAR data

(A) Chemical structure of isopomiferin and five analogs, ranked by potency in cell viability assays.

(B) Dose-response curves of SK-N-Be2 cells treated with isopomiferin analogs for 72 h. Data represent the mean from three replicate experiments, and error bars represent standard deviation across experiments (mean ± S.D.).

(C) MYCN abundance in SK-N-Be2 cells treated with isopomiferin, pomiferin, pomiferin dimethyl ether, or hydrogenated pomiferin for 24 h.

(D) Western blot analysis of MYCN and TEAD4 abundance in SK-N-Be2 cells following treatment with pomiferin for 24 h.

(E) Western blot analysis of MYCN abundance in SK-N-Be2 cells following treatment with 10 μM pomiferin across time.

(F) Transcript abundance of three direct targets of MYCN associated with poor patient outcome. SK-N-Be2 cells treated with 10 μM pomiferin for indicated time point. Values represent mean ± S.D. of three biological replicates.

activity and found the compound could bind mTOR kinase.[24] mTOR forms the kinase subunit of two separate complexes (mTORC1/2) that regulate cell proliferation in response to intrinsic and environmental cues.[25] Phosphorylation of $P70^{S6K}$ is a marker for mTORC1 activity, whereas phosphorylation of AKT (Ser473) (Ak strain transforming) serves as a signaling output for mTORC2.[26] Isopomiferin inhibited phosphorylation of $P70^{S6K}$, as well as the IGF1-induced phosphoactivation of AKT (Ser473), suggesting that signaling through both mTORC1/2 was attenuated (Figures 3D and 3E). However, treatment with the mTORC1 inhibitor rapamycin failed to invert the MR activity signature or to recapitulate isopomiferin's protein activity signature (Figure 3F). Together, these findings suggest that isopomiferin may disrupt mTORC1 in cells, but likely this is a dispensable aspect of isopomiferin's activity, at least in terms of MYCN inhibition, and that other targets are likely responsible for collapsing the MYCNA TCM.

Testing structural analogs reveals an isoflavonoid with improved potency

Isopomiferin is a prenylated isoflavonoid derived from extracts of the wild citrus species *Maclura pomifera*,[27,28] with chemical properties that make it an appealing scaffold for further development. The compound has low molecular weight, and is compliant with Lipinski's "Rule-of-Five" for optimal drug properties in humans.[29] Furthermore, the scaffold is amenable to modification by semi-synthesis and total synthesis to produce analogs for lead optimization. Isopomiferin was not particularly potent in cell-based assays, so we embarked on an optimization strategy to develop a more potent analog to enable *in vivo* tumor suppression.

In an effort to identify a potent analog of isopomiferin, we assembled a small collection of structurally related analogs and tested them in SK-N-Be2 cells. These compounds were collected from commercial vendors, isolated from natural sources, or are unique products created through semi-synthesis using the pomiferin scaffold as starting material. Remarkably, subtle structural modifications resulted in profound changes in MYCN inhibition and cell viability (Figures 4A–4C, S2A, and S2B). Notably, conversion of hydroxy functional groups on the phenyl ring to methoxy groups abrogated activity of the molecule, possibly by disrupting the ability to form hydrogen bonds with a protein target. Comparing the activity of six closely related structural analogs revealed pomiferin as the most potent

Please cite this article in press as: Stokes et al., Subtype-selective prenylated isoflavonoids disrupt regulatory drivers of MYCN-amplified cancers, Cell Chemical Biology (2023), https://doi.org/10.1016/j.chembiol.2023.11.007

compound of the group (Figure 4B). A broader panel of various flavonoid and isoflavonoid structures confirmed that pomiferin stood out as a potent inhibitor of cell viability (Figure S2C).

To assess the relationship between the inhibition of cell viability and MYCN abundance, we compared the ability of four closely related isoflavonoids to suppress MYCN abundance and induce cell death. Cells were treated with either isopomiferin, pomiferin, a hydrogenated version of pomiferin with reduced aromatic ring structures, or the inactive pomiferin dimethyl ether. Consistent with their effect on cell viability, pomiferin was the most potent compound and depleted both MYCN and TEAD4 at concentrations as low as 1.5 μM, within 6 h of treatment (Figures 4D and 4E). Isopomiferin and hydrogenated pomiferin had similar effects on MYCN abundance, although hydrogenated pomiferin was slightly more active at 5 μM. In contrast, and consistent with its inactivity, pomiferin dimethyl ether had no effect on MYCN abundance at concentrations tested. We evaluated the effect of pomiferin on transcript accumulation of three MYCN targets associated with poor outcome in NBL, including *PLK1*, *LIN28B*, and *BMI1*.[30–32] By 24 h, all three downstream targets were significantly reduced at the transcript level (Figure 4F), confirming that pomiferin is sufficient to disrupt oncogenic signaling through the MYCN-TEAD4 regulatory axis.

Casein kinase 2a inhibition contributes to MYCN depletion by prenylated isoflavonoids

To uncover kinase targets of isopomiferin and its functional analogs, we developed the virtual-inference of kinase inhibiton by gene regulatory networks (VIKING), an algorithm to enable data-driven inference of drug targets based on activity dysregulation of PPIs. Specifically, the VIKING algorithm uses gene regulatory networks inferred by the ARACNe algorithm[33,34] as input for VIPER to infer a comprehensive transcriptional and post-translational footprint of a drug's activity for >6,000 proteins with regulatory or signaling activity. These drug perturbation protein activity profiles are then used as input for the DeMAND algorithm (determination of mechanism of action by network dysregulation),[35] which is then used to evaluate PPI network dysregulation to help elucidate the full complement of cellular pathways that mediate a compound's pharmacological activity (Figure S3).

While VIPER is based on transcriptional regulation network analysis, VIKING also leverages PPI networks from the PrePPI database[36] to link signal transduction proteins including kinases, ubiquitin ligases, etc., with transcriptional regulators. Specifically, VIKING integrates DeMAND-based candidate MoA protein with VIPER-inferred effectors of drug activity, with negative NES scores representing drug-mediated loss of protein activity due to potentially direct chemical inhibition (see STAR methods). This list is filtered for human kinases to prioritize them as candidate compound targets (Figure S3). As a result, VIKING produced a list of potential cellular mechanisms of action of isopomiferin (Figure 5A), which were subsequently evaluated as potential direct targets of the compound. To benchmark the algorithm, we used CRISPR knockout and RNAi screening data as released by the Broad Institute Cancer Dependency Map (DepMap). Briefly, we built a receiver operating characteristic (ROC) curve using VIKING predictions on isopomiferin drug perturbations over SK-N-Be2 cells (n = 12 treatments and n = 6 controls) and compared them against gene dependency scores on SK-N-Be2 cells, integrated across the two platforms (i.e., CRISPR and RNAi) to control for technology bias. The area under the ROC (AUROC) computed with this approach is 70.8%, with ~50% sensitivity at ~95% specificity (Figure S3E).

VIKING predicted multiple kinases as cellular mechanisms of action for isopomiferin (Figure 5A), including cyclin dependent kinases (CDK2/CDK6), Polo-like kinase-1 (PLK1), both CK2 subunits α and α' (CSNK2A1/CSNK2A2), and aurora kinase A and B (AURKA/AURKB). These kinases had previously been found to have either physical or functional interactions with MYC. For example, CDK2 inhibition is synthetically lethal in MYCNA cell lines,[37] and PLK1 inhibition showed strong antitumor activity in MYCNA NBL preclinical models.[38,39] Reduced signaling through these pathways could also be an artifact of decreased cellular proliferation induced by the compound, so we prioritized this shortlist of potential targets by focusing on kinases that act upstream of MYC. Of these, CSNK2a1, which encodes for the catalytic subunit of CK2 phosphorylates cMYC and MYCN[40,41] proteins and can regulate their activity through indirect mechanisms.[14] CK2 is a pleiotropic kinase that phosphorylates multiple proteins that drive cell proliferation and support pro-survival mechanisms.[15,16] Previous studies have demonstrated that CK2 is inhibited by flavonoids, so we decided to test whether CK2 inhibition by the isoflavonoids could be mediating response to isopomiferin and pomiferin.[42]

Cell-free biochemical assays were used to test whether CK2a1 subunit was inhibited by isoflavonoids. Both isopomiferin and pomiferin inhibited CK2a1 kinase activity in a concentration-dependent manner (Figure 5B), albeit less potently than a CK2a-specific kinase inhibitor in development (CX-4945; silmitasertib). We tested whether pomiferin could suppress signaling through CK2 in cells by evaluating its effect on PTEN (Phosphatase and TENsin homolog deleted on chromosome 10) phosphorylation (Ser366), a downstream target of CK2 signaling. Treatment with either pomiferin or CX-4945 reduced phosphor-PTEN(ser366) levels, supporting the hypothesis that CK2 activity is attenuated by pomiferin (Figure 5C). Intriguingly, the potency of CX-4945 that was observed in the biochemical assays did not translate to cellular assays, and pomiferin was better able to suppress signaling through CK2 in cells compared to CX-4945.

The functional relationship between CK2 and MYCN was assessed by knocking down both CK2 alpha subunits and evaluating MYCN stability, hypothesizing that co-knockdown would destabilize MYCN similar to isoflavonoid treatment. siRNAs targeting CK2a1 and CK2a2 were pooled and transfected into SK-N-Be2 cells, followed by western blot and qPCR to confirm sufficient knockdown of both isoforms (Figures 5D and S4A). As with isoflavonoid treatment, knocking down CK2a1/2 suppresses MYCN protein, suggesting that the combined activity of the two subunits stabilizes MYCN. CK2a1 was further validated as a functional target of pomiferin by expressing a mutant isoform of CK2a1 harboring amino acid substitutions at residues essential for interaction with CX-4945.[15] Despite considerable effort, we were only able to achieve minimal plasmid transfection efficiency, which is an inherent challenge of NBL cell models. Despite this, cells expressing the mutant CK2 isoform conferred resistance to both pomiferin and CX-4945, while cells

Please cite this article in press as: Stokes et al., Subtype-selective prenylated isoflavonoids disrupt regulatory drivers of MYCN-amplified cancers, Cell Chemical Biology (2023), https://doi.org/10.1016/j.chembiol.2023.11.007

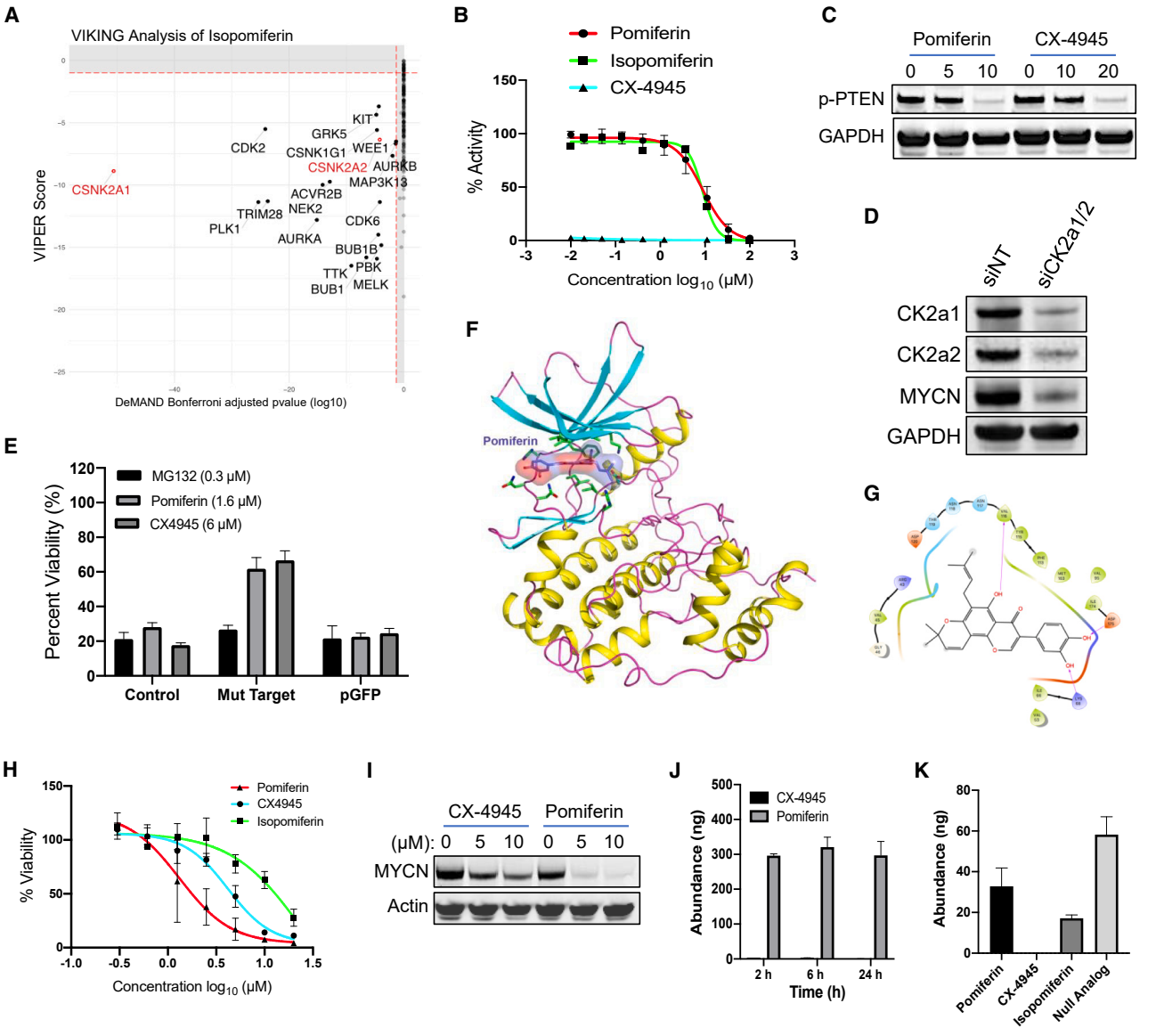

Figure 5. Prenylated isoflavonoids are cell permeable kinase inhibitors that act in part through CK2 inhibition

(A) VIKING output of predicted kinases targeted by isopomiferin.

(B) Cell free CK2a1 kinase activity in presence of pomiferin, isopomiferin or CX-4945. Values represent mean ± S.D. of three technical replicates.

(C) Western blot analysis of PTEN phosphorylation (Thr366) following treatment with either pomiferin or CX-4945 for 24 h.

(D) Western blot analysis of MYCN and two CK2a isoforms following siRNA-mediated knock-down of CK2a1/2 for 48 h in SK-N-Be2 cells.

(E) Cell viability of SK-N-Be2 cells expressing mutant CK2 isoform with impaired binding to inhibitor. Bars represent mean ± S.D. of three biological replicates.

(F) Crystal structure of human *apo* CK2a1. Cartoon representation of the human CK2a1 protomer for which a-helices, b-strands, and loops are colored in yellow (for Ca carbons), cyan, and light magenta, respectively. The modeled pomiferin (purple for Ca carbons) and side chains (green) of amino acids, which are predicted to interact with pomiferin are shown with stick models.

(G) Ligand interaction diagram of pomiferin in the crystal structure of CK2a1, corresponding to the docking pose shown in (F); arrows indicate hydrogen bonds.

(H) SK-N-Be2 cell viability following treatment with pomiferin, isopomiferin or CX-4945 for 72 h. Bars represent mean ± S.D. of three biological replicates.

(I) MYCN abundance following treatment with pomiferin or CX-4945 for 24 h.

(J) Cellular accumulation of pomiferin or CX-4945 for indicated time points. Values represent mean ± S.D. of three replicate experiments.

(K) Quantification of cellular abundance following treatment with prenylated isoflavonoids and CX-4945. Cell samples treated with 10 μM for 3 h, followed by LC-MS analysis. Values represent mean ± S.D. of three replicate experiments.

transfected with a GFP-expressing plasmid were not affected (Figure 5E). To assess the specificity of this response, the proteasome inhibitor MG132 was tested alongside the two compounds, yet no resistance was conferred by the plasmid. Together, these findings support the hypothesis that CK2a is a target of isoflavonoids in MYCNA NBL, and that both CX-4945 and pomiferin likely target similar residues on the CK2a1 protein binding site.

Please cite this article in press as: Stokes et al., Subtype-selective prenylated isoflavonoids disrupt regulatory drivers of MYCN-amplified cancers, Cell Chemical Biology (2023), https://doi.org/10.1016/j.chembiol.2023.11.007

Molecular modeling predicted the direct interaction between pomiferin and CK2a1, suggesting a possible molecular basis for the inhibition of kinase activity. The keto and hydroxyl groups of the isoflavone core are in hydrogen bonding proximity to the hinge region Val116 and make key interactions with it (Figures 5F and 5G). The hydroxyl groups of the phenyl ring interact with Lys68 and Asp175, consistent with the decrease in activity of the O-methyl analogs. The isoprene portions of the molecule are solvent exposed, consistent with the retention of activity on reduction of their double bonds. In addition, reduction of the double bond in the isoflavone ring, while slightly changing the shape of the molecule, allows it to maintain the key binding interactions. The crystal structure of CX-4945 reveals similar key hydrogen bonding interactions to CK2 to those found by docking studies with pomiferin. The carboxyl group of CX-4945 interacts with Lys68 and Asp175 and form hydrogen bonds between the pyridine nitrogen of CX-4945 and the hinge Val116.[43]

CX-4945, pomiferin, and isopomiferin were then tested in cell-based viability assays. Dose-response curves of SK-N-Be2 cells treated with the three compounds revealed pomiferin as the most potent inhibitor of viability, followed by CX-4945 and isopomiferin (Figure 5H). Pomiferin was also a more potent MYCN suppressor and apoptosis inducer than CX-4945, as evidenced by PARP and caspase3 cleavage (Figures 5I and S4B). These cell viability data are in contrast with biochemical data that demonstrated potent inhibition of CK2a by CX-4945, which has a reported K_i in the single-digit nanomolar range.[44] This discrepancy between cell-based and biochemical assays led to the hypothesis that differences in cell permeability are driving the differential activities observed between CX-4945 and the prenylated isoflavonoids.

To assess whether changes in cellular accumulation underpin differential activity between cell-based and biochemical assays, cells were treated with pomiferin or CX-4945 and cellular abundance of the compounds was determined by liquid chromatography-mass spectrometry (LC-MS). We initially confirmed the ability to detect and quantify pomiferin and CX-4945 by running standard samples of compound added directly to acetonitrile and injected into the LC-MS, which confirmed that both compounds ionized readily and were detectable on the instrument (Figure S4C). SK-N-Be2 cells were treated with 20 μM of CX-4945 or pomiferin and sampled across time. Pomiferin readily accumulated in cells, as ~300 ng of compound was detected in a sample of 2x10^6 cells (Figure 5J). Contrary to this, only 2.2 ng of CX-4945 was detected by 6 h, indicating that the CX-4945 compound may suffer from poor cell permeability. CX-4945 contains a carboxylic acid group, which is likely charged at physiological pH, which might impair cell permeability. Cell permeability could be a feature of pomiferin that enables the isoflavonoid to outperform CX-4945 in cell-based assays. Permeability was then compared between pomiferin, isopomiferin and the null analog pomiferin dimethyl ether. Pomiferin exhibited approximately twice the cellular accumulation of isopomiferin, consistent with its relative potency (Figure 5K). The null analog accumulated the most of all compounds tested, confirming that the loss of activity is not driven by poor cell permeability.

To further explore the cellular response to prenylated isoflavonoids, SK-N-Be2 cells were treated with pomiferin, isopomiferin, or the inactive analog pomiferin dimethyl ether for 24 h and evaluated by RNA sequencing (RNA-seq). As pomiferin dimethyl ether does not suppress MYCN, it was used as a negative control compound to evaluate unique chemical activity of the active analogs that could lead to MYCN suppression. VIPER analysis of top 25 MYCNA MRs confirmed that pomiferin suppressed a broader set of proteins than isopomiferin, when both compared to pomiferin null analog (Figure S5A). OncoTreat analysis of the same drug signatures suggests that pomiferin is more effective that isopomiferin in reverting the MYCNA TCM (Figure S5B). Moreover, VIKING analysis of pomiferin RNA-seq samples recapitulates CK2a1 as compound MoA (Figure S5C). Next, we used a PLATE-Seq perturbational screening on SK-N-Be2 cells to evaluate pomiferin analogs and other compounds with known MoA that target MYCNA-related pathways.[7,45–47] OncoTreat analysis identified pomiferin triacetate as top MR-inverter compound among selected pomiferin analogs (Figure S6A). Compounds that strongly reverted MYCNA MR signature are among pomiferin analogs and show similar protein activity profiles (Figure S6B), highlighting conserved activity across the series that is distinct from other compounds tested.

Pomiferin suppresses tumor growth *in vivo*

In vitro metabolic stability assays were initially performed to assess suitability for *in vivo* studies. Both compounds were incubated alongside a positive control compound (ferrostatin-1) in mouse plasma for 4 h and quantified by LC-MS. Isopomiferin was completely stable in mouse plasma, while approximately 75% pomiferin remained following incubation (Figure 6A). Similarly, both pomiferin and isopomiferin were reasonably stable to metabolic activation by mouse liver microsomes. Approximately ~80% pomiferin and ~50% isopomiferin remained after 2 h incubation, while the positive control compounds 7-ethoxycoumarin was metabolized across the duration of the assay, suggesting that prenylated isoflavonoids are metabolically stable in mice (Figure 6B).

The ability of the compounds to inhibit growth of MYCNA tumor xenografts was evaluated by treating tumor-bearing mice with daily intraperitoneal (i.p.) injections of 20 mg/kg isopomiferin or pomiferin. Mice that received daily treatments of pomiferin exhibited significantly decreased tumor volume compared to the vehicle-only control arm (Figure 6C). Mice treated with isopomiferin trended toward having smaller tumors than control groups, but these differences were not significant (Figures 6D and S7A). MYCN abundance was evaluated mid-experiment, following 14 days of treatment. Tumors were sampled 3 h post-dose on the fourteenth day of treatment. Pomiferin caused a substantial decrease in MYCN protein in tumors, relative to both vehicle-only and isopomiferin treated animals (Figure 6E). No differences in mean body weight were observed, suggesting that the treatments were well tolerated (Figure 6F).

Pomiferin suppresses MYC proteins across cancer cell line models

Genomic amplification of *MYCN* is commonly associated with aggressive NBL, but MYCN dysregulation has been observed in other aggressive tumors,[48] including Wilms' tumor (WT),[49] neuroendocrine prostate cancer (NEPC),[50,51] and lung cancers.[52,53] To identify non-NBL cell lines with dysregulated *MYCN*, expression profiles of >1000 cell lines from the cancer cell line encyclopedia

Please cite this article in press as: Stokes et al., Subtype-selective prenylated isoflavonoids disrupt regulatory drivers of MYCN-amplified cancers, Cell Chemical Biology (2023), https://doi.org/10.1016/j.chembiol.2023.11.007

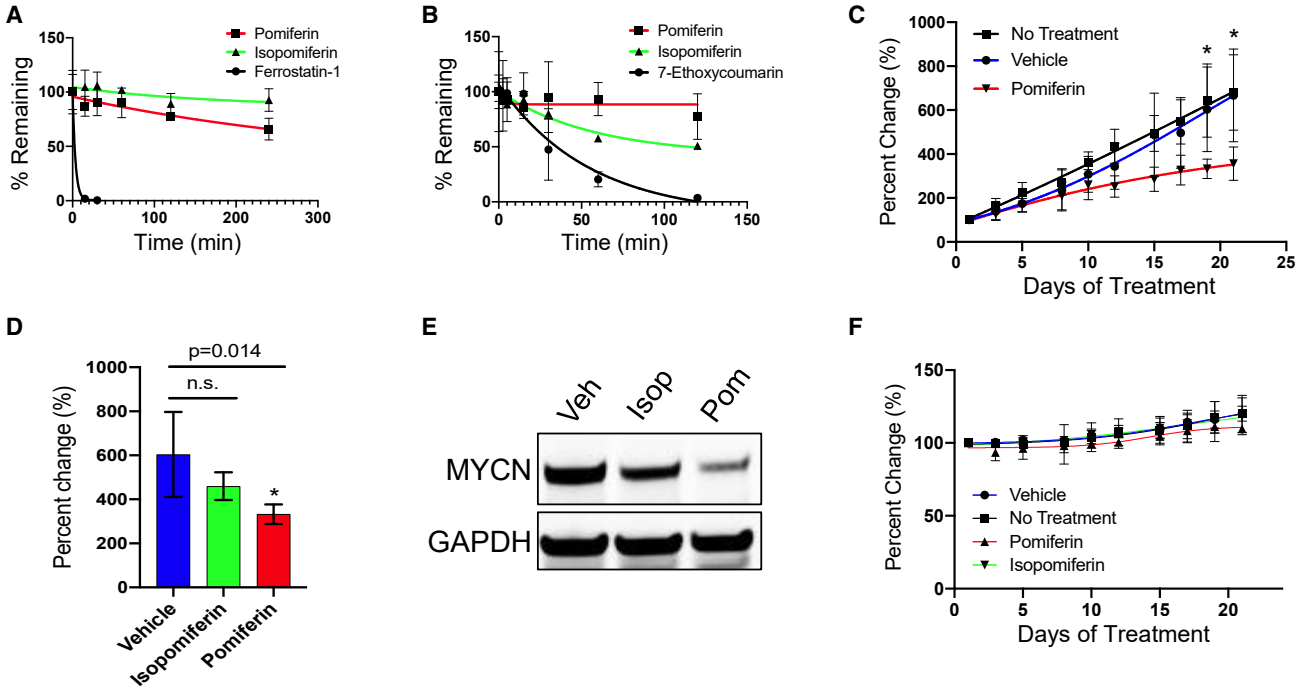

Figure 6. Pomiferin delays NBL tumor growth in mouse xenografts

(A) Stability of pomiferin isopomiferin and ferrostatin-1 (positive control) in mouse plasma across 4 h. Data represent mean ± S.D. of three replicates.

(B) Stability of isopomiferin, pomiferin and 7-ethoxycoumarin (positive control) following 2 h incubation in mouse liver microsomes at 0.5 mg/mL. Data represent mean ± S.D. of three replicates.

(C) Tumor growth across 21 days of treatment with 20 mg/kg pomiferin or vehicle control. Student's t test was performed to assess differences between vehicle and treatment groups; * indicates statistical significance at $p < 0.05$, n = 6 animals per group. Data represent mean ± S. D.

(D) Relative volume from mice treated with either isopomiferin (20 mg/kg), pomiferin (20 mg/kg), or vehicle control for 21 days.

(E) Western blot analysis of MYCN in SK-N-Be2 xenografts treated with vehicle, isopomiferin (20 mg/kg) or pomiferin (20 mg/kg) for 14 days.

(F) Mouse body weight across time, following daily treatment with isopomiferin (20 mg/kg), pomiferin (20 mg/kg), or vehicle control for 21 days.

(CCLE) were ranked based on *MYCN* transcript abundance. Twelve of the top fourteen cell lines were NBL, while the other two cell lines were derived from small cell lung cancer (SCLC; Figure S7B). Approximately 20% of SCLC tumors are associated with amplification of MYC family of proto-oncogenes,[53] and finding that these cell lines among the top ranked reflects this.

Pomiferin sensitivity was evaluated in two MYCN-driven SCLC cell lines (NCI-H69 and NCI-H526) and two cMYC-driven lung cancer models (A549 and NCI-H441). Similar to observations in NBL, cell lines with aberrant *MYCN* expression were more sensitive to pomiferin (Figure 7A). To test whether this was associated with MYCN depletion, NCI-H69 cells were treated with isopomiferin for 24 h, which resulted in concentration-dependent decrease in MYCN protein, albeit with less potency in the lung cancer lines relative to NBL (Figure 7B).

We hypothesized that pomiferin may deplete MYC proteins in general, and that cMYC and MYCL could also be suppressed by isoflavonoids. This is important in NBL since aberrant cMYC activity replaces that of MYCN in a subset of MYCNA-subtype tumors that are not MYCN amplified.[54] The ability of pomiferin to suppress cMYC in the cMYC-driven NBL line Sy5y was tested, which revealed inhibition of protein abundance similar to that observed in MYCNA NBL (Figure 7C). We then tested whether isoflavonoid could similarly suppress cMYC or MYCL in SCLC lung cancer cell lines, by treating NCI-H69 and NCI-H209 with isopomiferin for 24 h. Isopomiferin abrogated MYC protein in both SCLC lines (Figures 7D and 7E), confirming its activity is not limited to NBL. cMYC enables lung cancer tumors to evade immune detection by suppressing expression of *CCL5*,[55] so we confirmed that isopomiferin was sufficient to suppress the cMYC signaling axis by observing rescue of CCL5 expression upon prolonged treatment with isopomiferin (Figure 7F).

MYCN and cMYC promote their own gene expression in a TEAD4-mediated positive autoregulatory feedback loop and suppress each other in MYCNA NBL.[56,57] This regulatory relationship results in NBL cell line models that express either MYCN or cMYC, depending on genetic background and tumor subtype.[58] We assessed the effect of pomiferin on *MYCN* expression and observed a time-dependent decrease of *MYCN* transcript, consistent with a loss of MYCN autoregulation (Figure S7C). *cMYC* transcript was induced by pomiferin in SK-N-Be2 cells, consistent with the antagonistic relationship between MYC family members and the derepression that can occur when MYCN depleted in cells. We tested whether this could lead to a compensatory mechanism by evaluating cMYC protein upon MYCN depletion. Despite finding that pomiferin induced *cMYC* transcript accumulation, there was no concomitant increase in cMYC protein observed (Figure S7D). Thus, pomiferin represents a treatment option that broadly disrupts MYC stability, may be applicable across all MYC-driven tumor types, and

Please cite this article in press as: Stokes et al., Subtype-selective prenylated isoflavonoids disrupt regulatory drivers of MYCN-amplified cancers, Cell Chemical Biology (2023), https://doi.org/10.1016/j.chembiol.2023.11.007

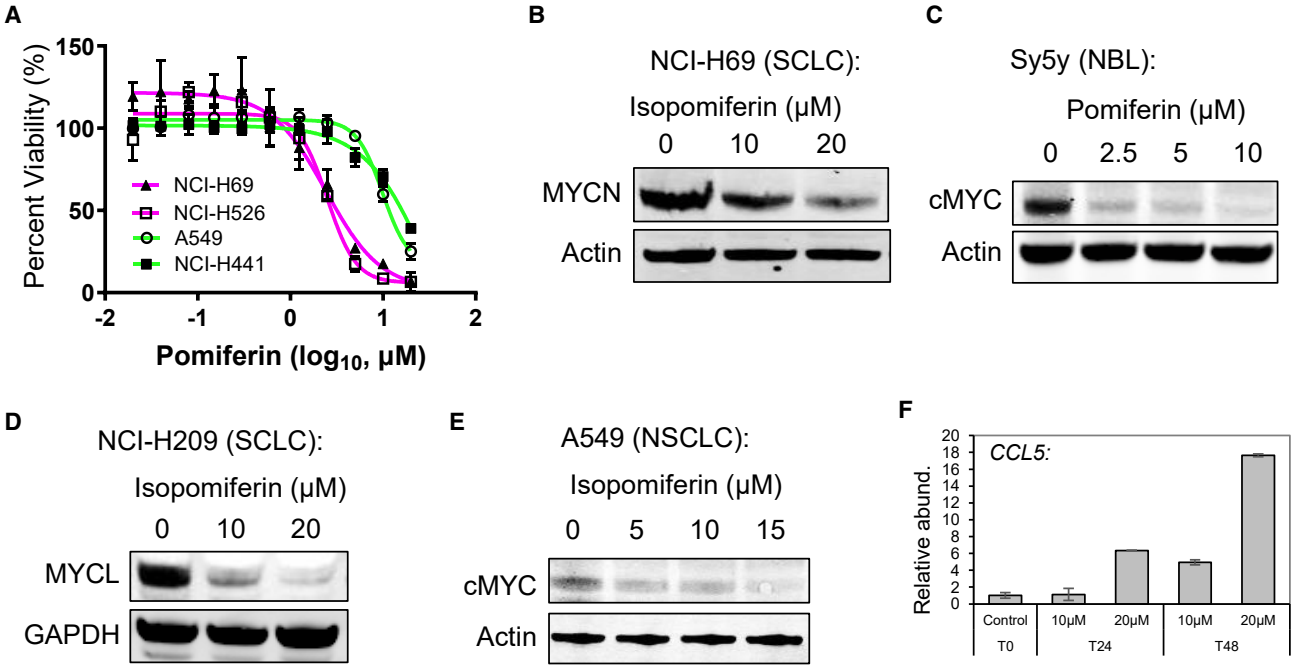

Figure 7. Prenylated isoflavones are active across MYC-driven cancers

(A) Cell viability assays from four lung cancer lines treated with pomiferin for 72 h. Data represent mean ± S.D. of three biological replicates.

(B) MYCN abundance measured in SCLC NCI-H69 cells treated with isopomiferin for 24 h.

(C) Western blot analysis of cMYC protein abundance Sy5Y NBL cells treated with pomiferin for 24 h.

(D) Western blot analysis of MYCL protein abundance NCI-H209 SCLC cells treated with isopomiferin for 24 h.

(E) cMYC abundance in NSCLC A549 cells treated with isopomiferin for 24 h.

(F) qPCR measurement of *CCL5* transcript in A549 cells following isopomiferin treatment for 48 h.

sidesteps possible compensatory mechanisms associated with MYCN-mediated cMYC inhibition.

DISCUSSION

The current standard of care for MYCNA NBL is grueling for pediatric patients and can have long-lasting implications for growth and development.[59,60] Children that receive high-dose radiotherapy and chemotherapy can often experience reduced growth rates throughput adolescence and higher incidence of hypothyroidism, ovarian failure, hearing loss and dental issues as adults.[59] A novel targeted therapy that disrupts core regulatory drivers of MYCNA NBL could improve clinical outcomes for patients and reduce the long-term health effects caused by current treatment modalities.

In this work we outline a proof-of-concept approach to the identification of "MR-inverting" agents that target the MYCNA TCM. Prenylated isoflavonoids are an interesting scaffold upon which future medicinal chemistry efforts can be focused, but optimization is required to develop these agents further. Identification of pomiferin presented a significant improvement in bioactivity over isopomiferin that enabled significant inhibition of SK-N-Be2 xenografts at 20 mg/kg in mice. Further improvements to the potency and solubility of these agents will likely enhance the antitumor activity and is the focus of ongoing research. Two studies highlight the therapeutic index for isoflavonoids, revealing that the anti-proliferative effect of pomiferin is >10-fold more potent against transformed cells relative to non-transformed cell line models.[27,61] If the isoflavonoids are selective for transformed cells, the agents may be well tolerated *in vivo* at higher doses. Consistent with this, finding that mouse body weight was unaffected by isopomiferin and pomiferin suggests these agents are tolerated in animals, but future toxicology studies are needed to evaluate this.

While CK2 inhibition appears central to the pomiferin mechanism of action, the potential for secondary targets as contributors to TCM collapse cannot be ruled out. Given that pomiferin treatment at micromolar concentrations is needed *in vitro* to suppress MYCN, it is likely that pomiferin interacts with secondary targets that may contribute to TCM collapse. A pomiferin analog with increased potency and selectivity would help elucidate the full extent of CK2's role in supporting the MYCNA TCM and help define the contribution of secondary targets to the mechanism of action. Identification of the inactive analog with no bioactivity is another useful tool that enables us to interrogate the mechanism of prenylated isoflavonoids. Targets that are inhibited in biochemical assays by the null analog can likely be dismissed as not relevant to pomiferin activity, and the compound serves as a negative control in expression profiling assays. Ongoing efforts are aimed at uncovering potential secondary targets that drive MYCNA TCM collapse by pomiferin.

CX-4945 is a potent CK2 inhibitor designed using *in silico* docking based methods and has shown activity in a variety of

Please cite this article in press as: Stokes et al., Subtype-selective prenylated isoflavonoids disrupt regulatory drivers of MYCN-amplified cancers, Cell Chemical Biology (2023), https://doi.org/10.1016/j.chembiol.2023.11.007

cancer models.[44,62,63] The compound received orphan designation status by the FDA, and is undergoing clinical testing for cholangiocarcinoma, and other tumors.[64] CX-4945 was used here to validate CK2 as a relevant target in MYCNA NBL, and to evaluate how prenylated isoflavonoids compare to CK2 inhibitors currently in development.[44,65] Despite single-digit nanomolar potency in biochemical assays, cellular activity of this inhibitor was not as potent as the prenylated isoflavonoids, suggesting that the scaffold has good chemical properties and cell-based activity upon which future lead optimization could be based. Given that NBL is a pediatric indication, the implications for targeting a pleiotropic kinase will need to be carefully considered, especially in the context of developmental effects.

The target patient population that can benefit from a novel MYCN-suppressing therapeutic extends beyond the MYCNA NBL patient group, which also includes cMYC-driven samples that lack the MYCN amplification event. Isopomiferin suppressed MYCN in lung cell lines, suggesting an MR-inverting therapeutic may benefit patients with a wide range of MYCN-driven tumors, independent of cancer type. For example, 12% of WT, NEPC, ~2–3% of non-small cell lung cancer (NSCLC), ~2–3% of liver cancers are MYCNA, representing a substantial patient population that could benefit from an isopomiferin-based therapeutic. This is particularly important because MYCN-driven tumors are noted for their aggressive phenotype and high mortality rate.[1] MYCN-amplification occurs in later stages of adult cancers to exacerbate tumor development at a time when patients have often exhausted other options.[48]

The development of PLATESeq and algorithms for its data analysis enables high-throughput and cost-effective screening to prioritize compounds based on disruption of cellular regulatory networks. While we have demonstrated the utility in MYCNA NBL, this approach can be readily adopted for cMYC-driven adult tumors. We have demonstrated that a limited screen of >5,000 molecules identified agents that disrupt the TCM and diminish MYC proteins across multiple cell-line models tested. Importantly, targeting MYC protein stability blocked the compensatory accumulation of other MYC family members, disrupting a plausible resistance mechanism to MYCN-targeting agents. In future, this method could be tailored to any MYC-driven tumors and applied to a more expansive chemical library in a targeted screening program to identify novel agents inhibiting core drivers of these aggressive tumors.

Limitations of the study

In this proof-of-concept study, we demonstrated a unique approach to interrogate the checkpoint module driving aggressive MYCNA NBL. As mentioned previously, CK2 is a key factor that defines the mechanism of prenylated isoflavonoids, yet other targets likely contribute to complete TCM collapse. A better understanding of secondary mechanisms would enable more refined medicinal chemistry efforts and the design of analogs with improved potency and selectivity. *In vivo*, SK-N-Be2 xenografts were sensitive to pomiferin at 20 mg/kg daily dosing, resulting in significant inhibition of tumor growth. Further optimization of dose regimen may improve the antitumor effects of pomiferin and other prenylated isoflavonoids. To this end, alternate dosing and administration strategies could be investigated to optimize exposure in tumor tissues, followed by pharmacokinetic/pharmacodynamic (PK/PD) analysis to validate effects *in vivo*. While preparing solutions for *in vivo* studies, it was noted that pomiferin solubility limited dosing at higher levels, which might be addressed through investigation of different formulation strategies. To improve translatability of findings, future studies could use more advanced tumor models, such as orthotopic models or patient derived xenografts.

SIGNIFICANCE

Subtype-selective chemical screening and high throughput expression profiling identified a development scaffold that ablates MYCN in cells and *in vivo*. By targeting regulatory circuits that stabilize MYCN protein expression, an indirect mechanism to inhibit the "undruggable" MYCN transcription factor was identified. Importantly, CK2 is a conserved mechanism that supports the MYC family of transcription factors, suggesting an opportunity for therapeutic MYC suppression across a variety of cancer contexts. MYC proteins are often amplified or hyperactive in cancer, and a small natural product with good tolerability is an opportunity to develop novel targeted therapies for some of the most aggressive tumors. This computational and experimental approach represents a promising new precision-oncology framework that can be generalized to elucidate targets and associated inhibitors across any cancer subtype.

STAR★METHODS

Detailed methods are provided in the online version of this paper and include the following:

- KEY RESOURCES TABLE
- RESOURCE AVAILABILITY
  - Lead contact
  - Materials availability
  - Data and code availability
- EXPERIMENTAL MODEL AND STUDY PARTICIPANT DETAILS
  - Mice
  - Cell lines
  - Cell lines and culture conditions
  - *In vivo* studies
- METHODS DETAILS
  - Chemical screening and cell viability assays
  - Protein detection by Western blot
  - RT-qPCR
  - PLATESeq cell culture, library prep, sequencing and analysis
  - Virtual-Inference of Kinase INhibiton by Gene regulatory networks algorithm
  - Quantification of cellular accumulation of compounds
  - Biochemical kinase assays
  - *In vitro* metabolic stability assays
  - Protein expression
  - Molecular modeling studies
  - Semi-synthesis of pomiferin and osajin analogs
  - Extraction of prenylated isoflavonoids from osage orange

- AZVII-13-1 (5,7-dihydroxy-3-(4-hydroxyphenyl)-6-(3-methylbut-2-en-1-yl)-4*H*-chromen-4-one)
- AZVII-13-2 (diprenylorobol; 3-(3,4-dihydroxyphenyl)-5,7-dihydroxy-6,8-bis(3-methylbut-2-en-1-yl)-4*H*-chromen-4-one)
- AZVII-13-3 (diprenylgenistein; 5,7-dihydroxy-3-(4-hydroxyphenyl)-6,8-bis(3-methylbut-2-en-1-yl)-4*H*-chromen-4-one)
- AZVII-12P (3-(3,4-dihydroxyphenyl)-5-hydroxy-6-isopentyl-8,8-dimethyl-2,3,9,10-tetrahydro-4*H*,8*H*-pyrano[2,3-*f*]chromen-4-one)
- AZVII-12O (5-hydroxy-3-(4-hydroxyphenyl)-6-isopentyl-8,8-dimethyl-2,3,9,10-tetrahydro-4*H*,8*H*-pyrano[2,3-*f*]chromen-4-one)
- AZVII-12-1 (3-(3,4-dihydroxyphenyl)-5,7-dihydroxy-6,8-diisopentylchroman-4-one)
- AZVII-12-2 (5,7-dihydroxy-3-(4-hydroxyphenyl)-6,8-diisopentylchroman-4-one)
- AZVII-89-11 3-(3,4-dimethoxyphenyl)-5-hydroxy-8,8-dimethyl-6-(3-methylbut-2-en-1-yl)-4*H*,8*H*-pyrano[2,3-*f*]chromen-4-one
- AZVI-89-12 5-hydroxy-3-(4-methoxyphenyl)-8,8-dimethyl-6-(3-methylbut-2-en-1-yl)-4*H*,8*H*-pyrano[2,3-*f*]chromen-4-one
- AZVII-4A (5-hydroxy-3-(3-hydroxy-4-methoxyphenyl)-8,8-dimethyl-6-(3-methylbut-2-en-1-yl)-4*H*,8*H*-pyrano[2,3-*f*]chromen-4-one)
- AZVII-44 4-(5-acetoxy-8,8-dimethyl-6-(3-methylbut-2-en-1-yl)-4-oxo-4*H*,8*H*-pyrano[2,3-*f*]chromen-3-yl)-1,2-phenylene diacetate

- QUANTIFICATION AND STATISTICAL ANALYSIS

SUPPLEMENTAL INFORMATION

Supplemental information can be found online at https://doi.org/10.1016/j.chembiol.2023.11.007.

ACKNOWLEDGMENTS

This work was supported by the National Cancer Institute (NCI) Cancer Target Discovery and Development program (U01CA217858 and U01CA272610 to A.C. and B.R.S.), NCI Cancer Systems Biology Consortium (U54CA209997 to A.C.), NCI Outstanding Investigator Awards (R35CA197745 to A.C. and R35CA209896 to B.R.S.), Shared Instrumentation Grants (S10OD012351 and S10OD021764 to A.C.), NCI P01CA087497 to B.R.S., a St. Baldrick's Foundation grant to B.R.S. This research was supported by a Young Investigator Award from the Swim Across America Foundation to M.E.S. A.V. was supported by a U.S. Department of Defense Early Investigator Research Award (W81XWH19-1-0337).

AUTHOR CONTRIBUTIONS

M.E.S.: conceptualization, methodology, validation, investigation, writing – review & editing. A.V.: conceptualization, methodology, software, formal analysis, visualization, writing – review & editing. J.C.S.: investigation. A.Z.: methodology, investigation, resources, writing – review & editing. E.R.: investigation. N.S.: investigation. Q.W.: investigation. J.D.: investigation. F.F.: investigation, resources. P.R.: investigation. A.C.: conceptualization, methodology, software, formal analysis, supervision, project administration, funding acquisition, writing – review & editing. B.R.S.: conceptualization, methodology, supervision, project administration, funding acquisition, writing – review & editing.

DECLARATION OF INTERESTS

B.R.S. is an inventor on patents and patent applications involving ferroptosis, holds equity in and serves as a consultant to Exarta Therapeutics, and ProJenX Inc, holds equity in Sonata Therapeutics, and serves as a consultant to Weatherwax Biotechnologies Corporation and Akin Gump Strauss Hauer & Feld LLP. B.R.S., M.E.S, A.Z., A.C., and A.V. are inventors on a patent application related to this work. A.C. is founder, equity holder, and consultant of DarwinHealth Inc., a company that has licensed some of the algorithms used in this manuscript from Columbia University. Columbia University is also an equity holder in DarwinHealth Inc.

Received: November 2, 2022
Revised: July 18, 2023
Accepted: November 13, 2023
Published: December 06, 2023

REFERENCES

1. Huang, M., and Weiss, W.A. (2013). Neuroblastoma and MYCN. Cold Spring Harb. Perspect Med. *3*, a014415.
2. Marshall, G.M., Carter, D.R., Cheung, B.B., Liu, T., Mateos, M.K., Meyerowitz, J.G., and Weiss, W.A. (2014). The prenatal origins of cancer. Nat. Rev. Cancer *14*, 277–289.
3. Brodeur, G.M., Seeger, R.C., Schwab, M., Varmus, H.E., and Bishop, J.M. (1984). Amplification of N-myc in untreated human neuroblastomas correlates with advanced disease stage. Science *224*, 1121–1124.
4. Seeger, R.C., Brodeur, G.M., Sather, H., Dalton, A., Siegel, S.E., Wong, K.Y., and Hammond, D. (1985). Association of multiple copies of the N-myc oncogene with rapid progression of neuroblastomas. N. Engl. J. Med. *313*, 1111–1116.
5. Øra, I., and Eggert, A. (2011). Progress in treatment and risk stratification of neuroblastoma: impact on future clinical and basic research. Semin. Cancer Biol. *21*, 217–228.
6. Richards, M.W., Burgess, S.G., Poon, E., Carstensen, A., Eilers, M., Chesler, L., and Bayliss, R. (2016). Structural basis of N-Myc binding by Aurora-A and its destabilization by kinase inhibitors. Proc. Natl. Acad. Sci. USA *113*, 13726–13731.
7. Gustafson, W.C., Meyerowitz, J.G., Nekritz, E.A., Chen, J., Benes, C., Charron, E., Simonds, E.F., Seeger, R., Matthay, K.K., Hertz, N.T., et al. (2014). Drugging MYCN through an allosteric transition in Aurora kinase A. Cancer Cell *26*, 414–427.
8. Rajbhandari, P., Lopez, G., Capdevila, C., Salvatori, B., Yu, J., Rodriguez-Barrueco, R., Martinez, D., Yarmarkovich, M., Weichert-Leahey, N., Abraham, B.J., et al. (2018). Cross-cohort analysis identifies a TEAD4 - MYCN positive-feedback loop as the core regulatory element of high-risk neuroblastoma. Cancer Discov. *8*, 582–599.
9. Califano, A., and Alvarez, M.J. (2017). The recurrent architecture of tumour initiation, progression and drug sensitivity. Nat. Rev. Cancer *17*, 116–130.
10. Alvarez, M.J., Subramaniam, P.S., Tang, L.H., Grunn, A., Aburi, M., Rieckhof, G., Komissarova, E.V., Hagan, E.A., Bodei, L., Clemons, P.A., et al. (2018). A precision oncology approach to the pharmacological targeting of mechanistic dependencies in neuroendocrine tumors. Nat. Genet. *50*, 979–989.
11. Bush, E.C., Ray, F., Alvarez, M.J., Realubit, R., Li, H., Karan, C., Califano, A., and Sims, P.A. (2017). PLATE-Seq for genome-wide regulatory network analysis of high-throughput screens. Nat. Commun. *8*, 105.
12. Mundi, P.S., Dela Cruz, F.S., Grunn, A., Diolaiti, D., Mauguen, A., Rainey, A.R., Guillan, K., Siddiquee, A., You, D., Realubit, R., et al. (2023). A Transcriptome-Based Precision Oncology Platform for Patient-Therapy Alignment in a Diverse Set of Treatment-Resistant Malignancies. Cancer Discov. *13*, 1386–1407.
13. Alvarez, M.J., Shen, Y., Giorgi, F.M., Lachmann, A., Ding, B.B., Ye, B.H., and Califano, A. (2016). Functional characterization of somatic mutations in cancer using network-based inference of protein activity. Nat. Genet. *48*, 838–847.

14. Wang, K., Saito, M., Bisikirska, B.C., Alvarez, M.J., Lim, W.K., Rajbhandari, P., Shen, Q., Nemenman, I., Basso, K., Margolin, A.A., et al. (2009). Genome-wide identification of post-translational modulators of transcription factor activity in human B cells. Nat. Biotechnol. *27*, 829–839.

15. Turowec, J.P., Duncan, J.S., French, A.C., Gyenis, L., St Denis, N.A., Vilk, G., and Litchfield, D.W. (2010). Protein kinase CK2 is a constitutively active enzyme that promotes cell survival: strategies to identify CK2 substrates and manipulate its activity in mammalian cells. Methods Enzymol. *484*, 471–493.

16. Litchfield, D.W. (2003). Protein kinase CK2: structure, regulation and role in cellular decisions of life and death. Biochem. J. *369*, 1–15.

17. Vasciaveo, A., Arriaga, J.M., de Almeida, F.N., Zou, M., Douglass, E.F., Picech, F., Shibata, M., Rodriguez-Calero, A., de Brot, S., Mitrofanova, A., et al. (2023). OncoLoop: A Network-Based Precision Cancer Medicine Framework. Cancer Discov. *13*, 386–409.

18. Stokes, M.E., Small, J.C., Vasciaveo, A., Shimada, K., Hirschhorn, T., Califano, A., and Stockwell, B.R. (2020). Mesenchymal subtype neuroblastomas are addicted to TGF-betaR2/HMGCR-driven protein geranylgeranylation. Sci. Rep. *10*, 10748.

19. Paull, E.O., Aytes, A., Jones, S.J., Subramaniam, P.S., Giorgi, F.M., Douglass, E.F., Tagore, S., Chu, B., Vasciaveo, A., Zheng, S., et al. (2021). A modular master regulator landscape controls cancer transcriptional identity. Cell *184*, 334–351.e20.

20. Shah, Z., Gohar, U.F., Jamshed, I., Mushtaq, A., Mukhtar, H., Zia-Ui-Haq, M., Toma, S.I., Manea, R., Moga, M., and Popovici, B. (2021). Podophyllotoxin: History, Recent Advances and Future Prospects. Biomolecules *11*, 603.

21. Kashyap, D., Mondal, R., Tuli, H.S., Kumar, G., and Sharma, A.K. (2016). Molecular targets of gambogic acid in cancer: recent trends and advancements. Tumour Biol. *37*, 12915–12925.

22. Liberzon, A., Birger, C., Thorvaldsdóttir, H., Ghandi, M., Mesirov, J.P., and Tamayo, P. (2015). The Molecular Signatures Database (MSigDB) hallmark gene set collection. Cell Syst. *1*, 417–425.

23. Gustafson, W.C., and Weiss, W.A. (2010). Myc proteins as therapeutic targets. Oncogene *29*, 1249–1259.

24. Bajer, M.M., Kunze, M.M., Blees, J.S., Bokesch, H.R., Chen, H., Brauss, T.F., Dong, Z., Gustafson, K.R., Biondi, R.M., Henrich, C.J., et al. (2014). Characterization of pomiferin triacetate as a novel mTOR and translation inhibitor. Biochem. Pharmacol. *88*, 313–321.

25. Kim, L.C., Cook, R.S., and Chen, J. (2017). mTORC1 and mTORC2 in cancer and the tumor microenvironment. Oncogene *36*, 2191–2201.

26. Sarbassov, D.D., Guertin, D.A., Ali, S.M., and Sabatini, D.M. (2005). Phosphorylation and regulation of Akt/PKB by the rictor-mTOR complex. Science *307*, 1098–1101.

27. Darji, K., Miglis, C., Wardlow, A., and Abourashed, E.A. (2013). HPLC Determination of Isoflavone Levels in Osage Orange from the Midwest and Southern United States. J. Agr. Food Chem. *61*, 6806–6811.

28. Wolfrom, M.L., Harris, W.D., Johnson, G.F., Mahan, J.E., Moffett, S.M., and Wildi, B. (1946). Osage Orange Pigments .11. Complete Structures of Osajin and Pomiferin. J. Am. Chem. Soc. *68*, 406–418.

29. Lipinski, C.A., Lombardo, F., Dominy, B.W., and Feeney, P.J. (2001). Experimental and computational approaches to estimate solubility and permeability in drug discovery and development settings. Adv. Drug Deliv. Rev. *46*, 3–26.

30. Ackermann, S., Goeser, F., Schulte, J.H., Schramm, A., Ehemann, V., Hero, B., Eggert, A., Berthold, F., and Fischer, M. (2011). Polo-Like Kinase 1 is a Therapeutic Target in High-Risk Neuroblastoma. Clin. Cancer Res. *17*, 731–741.

31. Cotterman, R., and Knoepfler, P.S. (2009). N-Myc regulates expression of pluripotency genes in neuroblastoma including lif, klf2, klf4, and lin28b. PLoS One *4*, e5799.

32. Huang, R., Cheung, N.K.V., Vider, J., Cheung, I.Y., Gerald, W.L., Tickoo, S.K., Holland, E.C., and Blasberg, R.G. (2011). MYCN and MYC regulate tumor proliferation and tumorigenesis directly through BMI1 in human neuroblastomas. Faseb. J. *25*, 4138–4149.

33. Lachmann, A., Giorgi, F.M., Lopez, G., and Califano, A. (2016). ARACNe-AP: gene network reverse engineering through adaptive partitioning inference of mutual information. Bioinformatics *32*, 2233–2235.

34. Basso, K., Margolin, A.A., Stolovitzky, G., Klein, U., Dalla-Favera, R., and Califano, A. (2005). Reverse engineering of regulatory networks in human B cells. Nat. Genet. *37*, 382–390.

35. Woo, J.H., Shimoni, Y., Yang, W.S., Subramaniam, P., Iyer, A., Nicoletti, P., Rodríguez Martínez, M., López, G., Mattioli, M., Realubit, R., et al. (2015). Elucidating Compound Mechanism of Action by Network Perturbation Analysis. Cell *162*, 441–451.

36. Zhang, Q.C., Petrey, D., Deng, L., Qiang, L., Shi, Y., Thu, C.A., Bisikirska, B., Lefebvre, C., Accili, D., Hunter, T., et al. (2012). Structure-based prediction of protein-protein interactions on a genome-wide scale. Nature *490*, 556–560.

37. Molenaar, J.J., Ebus, M.E., Geerts, D., Koster, J., Lamers, F., Valentijn, L.J., Westerhout, E.M., Versteeg, R., and Caron, H.N. (2009). Inactivation of CDK2 is synthetically lethal to MYCN over-expressing cancer cells. Proc. Natl. Acad. Sci. USA *106*, 12968–12973.

38. Xiao, D., Yue, M., Su, H., Ren, P., Jiang, J., Li, F., Hu, Y., Du, H., Liu, H., and Qing, G. (2016). Polo-like Kinase-1 Regulates Myc Stabilization and Activates a Feedforward Circuit Promoting Tumor Cell Survival. Mol. Cell *64*, 493–506.

39. Pajtler, K.W., Sadowski, N., Ackermann, S., Althoff, K., Schönbeck, K., Batzke, K., Schäfers, S., Odersky, A., Heukamp, L., Astrahantseff, K., et al. (2017). The GSK461364 PLK1 inhibitor exhibits strong antitumoral activity in preclinical neuroblastoma models. Oncotarget *8*, 6730–6741.

40. Lüscher, B., Kuenzel, E.A., Krebs, E.G., and Eisenman, R.N. (1989). Myc Oncoproteins Are Phosphorylated by Casein Kinase-Ii. EMBO J. *8*, 1111–1119.

41. Hagiwara, T., Nakaya, K., Nakamura, Y., Nakajima, H., Nishimura, S., and Taya, Y. (1992). Specific Phosphorylation of the Acidic Central Region of the N-Myc Protein by Casein Kinase-Ii. Eur. J. Biochem. *209*, 945–950.

42. Baier, A., Galicka, A., Nazaruk, J., and Szyszka, R. (2017). Selected flavonoid compounds as promising inhibitors of protein kinase CK2 alpha and CK2 alpha', the catalytic subunits of CK2. Phytochemistry *136*, 39–45.

43. Ferguson, A.D., Sheth, P.R., Basso, A.D., Paliwal, S., Gray, K., Fischmann, T.O., and Le, H.V. (2011). Structural basis of CX-4945 binding to human protein kinase CK2. FEBS Lett. *585*, 104–110.

44. Siddiqui-Jain, A., Drygin, D., Streiner, N., Chua, P., Pierre, F., O'Brien, S.E., Bliesath, J., Omori, M., Huser, N., Ho, C., et al. (2010). CX-4945, an Orally Bioavailable Selective Inhibitor of Protein Kinase CK2, Inhibits Prosurvival and Angiogenic Signaling and Exhibits Antitumor Efficacy. Cancer Res. *70*, 10288–10298.

45. Galiger, C., Dahlhaus, M., Vitek, M.P., Debatin, K.M., and Beltinger, C. (2022). PPP2CA Is a Novel Therapeutic Target in Neuroblastoma Cells That Can Be Activated by the SET Inhibitor OP449. Front. Oncol. *12*, 744984.

46. Guo, Y., Guo, D., Zhang, S., Zhang, Y., He, X., Jiang, X., Chan, A.M., Zou, L., Sun, J., and Zhao, H. (2022). Inhibition of PI3 kinase isoform p110alpha suppresses neuroblastoma growth and induces the reduction of Anaplastic Lymphoma Kinase. Cell Biosci. *12*, 210.

47. Puissant, A., Frumm, S.M., Alexe, G., Bassil, C.F., Qi, J., Chanthery, Y.H., Nekritz, E.A., Zeid, R., Gustafson, W.C., Greninger, P., et al. (2013). Targeting MYCN in neuroblastoma by BET bromodomain inhibition. Cancer Discov. *3*, 308–323.

48. Rickman, D.S., Schulte, J.H., and Eilers, M. (2018). The Expanding World of N-MYC-Driven Tumors. Cancer Discov. *8*, 150–163.

49. Williams, R.D., Chagtai, T., Alcaide-German, M., Apps, J., Wegert, J., Popov, S., Vujanic, G., van Tinteren, H., van den Heuvel-Eibrink, M.M., Kool, M., et al. (2015). Multiple mechanisms of MYCN dysregulation in Wilms tumour. Oncotarget *6*, 7232–7243.

50. Lee, J.K., Phillips, J.W., Smith, B.A., Park, J.W., Stoyanova, T., McCaffrey, E.F., Baertsch, R., Sokolov, A., Meyerowitz, J.G., Mathis, C., et al. (2016). N-Myc Drives Neuroendocrine Prostate Cancer Initiated from Human Prostate Epithelial Cells. Cancer Cell *29*, 536–547.

51. Beltran, H., Prandi, D., Mosquera, J.M., Benelli, M., Puca, L., Cyrta, J., Marotz, C., Giannopoulou, E., Chakravarthi, B.V.S.K., Varambally, S., et al. (2016). Divergent clonal evolution of castration-resistant neuroendocrine prostate cancer. Nat. Med. *22*, 298–305.

52. Wong, A.J., Ruppert, J.M., Eggleston, J., Hamilton, S.R., Baylin, S.B., and Vogelstein, B. (1986). Gene Amplification of C-Myc and N-Myc in Small Cell-Carcinoma of the Lung. Science *233*, 461–464.

53. Brägelmann, J., Böhm, S., Guthrie, M.R., Mollaoglu, G., Oliver, T.G., and Sos, M.L. (2017). Family matters: How MYC family oncogenes impact small cell lung cancer. Cell Cycle *16*, 1489–1498.

54. Rajbhandari, P., Lopez, G., Capdevila, C., Salvatori, B., Yu, J., Rodriguez-Barrueco, R., Martinez, D., Yarmarkovich, M., Weichert-Leahey, N., Abraham, B.J., et al. (2018). Cross-Cohort Analysis Identifies a TEAD4-MYCN Positive Feedback Loop as the Core Regulatory Element of High-Risk Neuroblastoma. Cancer Discov. *8*, 582–599.

55. Topper, M.J., Vaz, M., Chiappinelli, K.B., DeStefano Shields, C.E., Niknafs, N., Yen, R.W.C., Wenzel, A., Hicks, J., Ballew, M., Stone, M., et al. (2017). Epigenetic Therapy Ties MYC Depletion to Reversing Immune Evasion and Treating Lung Cancer. Cell *171*, 1284–1300.e21.

56. Suenaga, Y., Kaneko, Y., Matsumoto, D., Hossain, M.S., Ozaki, T., and Nakagawara, A. (2009). Positive auto-regulation of MYCN in human neuroblastoma. Biochem. Biophys. Res. Commun. *390*, 21–26.

57. Breit, S., and Schwab, M. (1989). Suppression of MYC by high expression of NMYC in human neuroblastoma cells. J. Neurosci. Res. *24*, 21–28.

58. Zimmerman, M.W., Liu, Y., He, S., Durbin, A.D., Abraham, B.J., Easton, J., Shao, Y., Xu, B., Zhu, S., Zhang, X., et al. (2018). MYC Drives a Subset of High-Risk Pediatric Neuroblastomas and Is Activated through Mechanisms Including Enhancer Hijacking and Focal Enhancer Amplification. Cancer Discov. *8*, 320–335.

59. Cohen, L.E., Gordon, J.H., Popovsky, E.Y., Gunawardene, S., Duffey-Lind, E., Lehmann, L.E., and Diller, L.R. (2014). Late effects in children treated with intensive multimodal therapy for high-risk neuroblastoma: high incidence of endocrine and growth problems. Bone Marrow Transplant. *49*, 502–508.

60. Laverdière, C., Liu, Q., Yasui, Y., Nathan, P.C., Gurney, J.G., Stovall, M., Diller, L.R., Cheung, N.K., Wolden, S., Robison, L.L., and Sklar, C.A. (2009). Long-term outcomes in survivors of neuroblastoma: a report from the Childhood Cancer Survivor Study. J. Natl. Cancer Inst. *101*, 1131–1140.

61. Son, I.H., Chung, I.M., Lee, S.I., Yang, H.D., and Moon, H.I. (2007). Pomiferin, histone deacetylase inhibitor isolated from the fruits of Maclura pomifera. Bioorg. Med. Chem. Lett. *17*, 4753–4755.

62. Prins, R.C., Burke, R.T., Tyner, J.W., Druker, B.J., Loriaux, M.M., and Spurgeon, S.E. (2013). CX-4945, a selective inhibitor of casein kinase-2 (CK2), exhibits anti-tumor activity in hematologic malignancies including enhanced activity in chronic lymphocytic leukemia when combined with fludarabine and inhibitors of the B-cell receptor pathway. Leukemia *27*, 2094–2096.

63. Chen, Y., Wang, Y., Wang, J., Zhou, Z., Cao, S., and Zhang, J. (2023). Share Strategies of Targeting CK2 in Drug Discovery: Challenges, Opportunities, and Emerging Prospects. J Med Chem *66*, 2257–2281.

64. Chon, H.J., Bae, K.J., Lee, Y., and Kim, J. (2015). The casein kinase 2 inhibitor, CX-4945, as an anti-cancer drug in treatment of human hematological malignancies. Front. Pharmacol. *6*, 70.

65. Anderes, K., Siddiqui-Jain, A., Streiner, N., Chua, P., Pierre, F., Omori, M., Darjarnia, L., Stansfield, R., Phung, J., Bliesath, J., et al. (2009). Discovery and characterization of CX-4945 a selective orally bioavailable small molecule inhibitor of protein kinase CK2: Phase 1 initiated. Cancer Res. *69*, 10288–10298.

66. Riley, J.W., Stouffer, S.A., Suchman, E.A., Devinney, L.C., Star, S.A., and Williams, R.M. (1949). The american soldier: Adjustment during army life. Am. Sociol. Rev. *14*, 557.

67. Manning, G., Whyte, D.B., Martinez, R., Hunter, T., and Sudarsanam, S. (2002). The protein kinase complement of the human genome. Science *298*, 1912–1934.

68. Welsch, M.E., Kaplan, A., Chambers, J.M., Stokes, M.E., Bos, P.H., Zask, A., Zhang, Y., Sanchez-Martin, M., Badgley, M.A., Huang, C.S., et al. (2017). Multivalent Small-Molecule Pan-RAS Inhibitors. Cell *168*, 878–889.e29.

69. Colletti, L.M., Liu, Y., Koev, G., Richardson, P.L., Chen, C.M., and Kati, W. (2008). Methods to measure the intracellular concentration of unlabeled compounds within cultured cells using liquid chromatography/tandem mass spectrometry. Anal. Biochem. *383*, 186–193.

70. Bos, P.H., Lowry, E.R., Costa, J., Thams, S., Garcia-Diaz, A., Zask, A., Wichterle, H., and Stockwell, B.R. (2019). Development of MAP4 Kinase Inhibitors as Motor Neuron-Protecting Agents. Cell Chem. Biol. *26*, 1703–1715.e37.

71. Wickham, H., Chang, W., and Wickham, M.H. (2016). Package 'ggplot2'. Create elegant data visualisations using the grammar of graphics. Version 2, pp. 1–189.

72. Wickham, H., Averick, M., Bryan, J., Chang, W., McGowan, L., François, R., Grolemund, G., Hayes, A., Henry, L., Hester, J., et al. (2019). Welcome to the Tidyverse. J. Open Source Softw. *4*, 1686.

Please cite this article in press as: Stokes et al., Subtype-selective prenylated isoflavonoids disrupt regulatory drivers of MYCN-amplified cancers, Cell Chemical Biology (2023), https://doi.org/10.1016/j.chembiol.2023.11.007

STAR★METHODS

KEY RESOURCES TABLE

REAGENT or RESOURCE	SOURCE	IDENTIFIER
Antibodies		
MYCN, Rabbit mAb	Cell Signaling Technology	Cat. # 84406, RRID:AB_2800038
CMYC, Rabbit mAb	Cell Signaling Technology	Cat. # 5605, RRID:AB_1903938
ACTIN, Mouse mAb	Cell Signaling Technology	Cat. # 3700, RRID:AB_10928322
Caspase, Rabbit mAb	Cell Signaling Technology	Cat. # 9662, RRID:AB_331439
PARP, Rabbit mAb	Cell Signaling Technology	Cat. # 5625, RRID:AB_10699459
GAPDH, Rabbit mAb	Cell Signaling Technology	Cat. # 5174, RRID:AB_10622025
TEAD4, Mouse mAb	Abcam	Cat. # ab58310, RRID:AB_945789
Chemicals, peptides, and recombinant proteins		
CX-4945	Selleckchem	Cat. #S2248
methylene blue	Sigma millipore	Cat. # 457250
fluvastatin	Sigma millipore	Cat. # SML0038
triamterene	Sigma millipore	Cat. #T4143
Imipramine HCl	Sigma millipore	Cat. #I7379
Candesartan cilexetil	Sigma millipore	Cat. # SML0245
Podofilotoxin	Sigma millipore	Cat. #P4405
Critical commercial assays		
CellTitreGlo	Promega	Cat. #G7573
Deposited data		
RNASeq profiling of treated SK-N-Be2 cells	This paper	GEO: GSE245006
PLATESeq data of chemical screening plate	This paper	GEO: GSE245006
PLATESeq data of SK-N-Be2 cells treated with isoflavonoids	This paper	GEO: GSE245006
PLATESeq data of SK-N-Be2 cells treated with compounds of known MoA (ure S6)	This paper	GEO: GSE245006
Achilles shRNA and CRISPR KO Data	DepMap; Broad Institute	https://depmap.org/portal/download/all/
Molecular Signatures Database (MSigDB)	Broad Institute	https://www.gsea-msigdb.org/gsea/msigdb/index.jsp
RNASeq from NBL tumors	NCI TARGET	dbGap: phs000467
Human kinases data	Manning et al.[67]	http://kinase.com/human/kinome/
Experimental models: Cell lines		
A-549	ATCC	RRID:CVCL_0023
IMR-32	ATCC	RRID:CVCL_0346
LAN-1	ATCC	RRID:CVCL_1827
NCI-H69	ATCC	RRID:CVCL_1579
NCI-H209	ATCC	RRID:CVCL_1525
NCI-H441	ATCC	RRID:CVCL_1561
NLF	ATCC	RRID:CVCL_E217
SK-N-AS	ATCC	RRID:CVCL_1700
SK-N-Be2	ATCC	RRID:CVCL_0528
SH-Sy5y	ATCC	RRID:CVCL_0019
SMS-SAN	ATCC	RRID:CVCL_7137
Oligonucleotides		
Primers used in qPCR experiments	This paper	Table S1
siCK2a1	Dharmacon	Cat. # L-003475-00-0010
siCK2a2	Dharmacon	Cat. # L-004752-00-0010
siNT	Dharmacon	Cat. # D-001810-10-05

(*Continued on next page*)

Please cite this article in press as: Stokes et al., Subtype-selective prenylated isoflavonoids disrupt regulatory drivers of MYCN-amplified cancers, Cell Chemical Biology (2023), https://doi.org/10.1016/j.chembiol.2023.11.007

Continued

REAGENT or RESOURCE	SOURCE	IDENTIFIER
Software and algorithms		
VIKING algorithm	This paper	https://github.com/alevax/VIKING
VIPER algorithm R package	Alvarez et al.[13]	https://doi.org/10.18129/B9.bioc.viper
PrePPI Interactome	Zhang et al.[36]	https://honiglab.c2b2.columbia.edu/PrePPI/index.html
ARACNe-AP algorithm	Lachmann et al.[33]	https://github.com/califano-lab/ARACNe-AP
ggplot2: Graphics for Data Analysis	Wickham et al.[71]	https://ggplot2.tidyverse.org/
Tidyverse R Package	Wickham et al.[72]	https://www.tidyverse.org/
GraphPad Prism	GraphPad Software Inc.	RRID:SCR_002798

RESOURCE AVAILABILITY

Lead contact

Further information and requests for resources and reagents should be directed to and will be fulfilled by the lead contact, Brent R Stockwell (bs2198@columbia.edu).

Materials availability

All reported compounds generated in this manuscript will be available upon reasonable request to the lead contact after completion of an MTA and as long as supplies are available. Detailed procedures for isolating pomiferin, osajin, diprenylgenistein, diprenylorobol, and AZVII 13-1 are included in section "extraction of prenylated isoflavonoids from osage orange" in STAR methods.

Data and code availability

- RNASeq and PLATESeq sequencing data have been uploaded to the gene expression omnibus (GEO) with accession number GEO: GSE245006, and are publicly available at the time of publication. Accession numbers are listed in the key resources table.
- All original code has been deposited at GitHub (https://github.com/alevax/VIKING) and is publicly available as of the date of publication. DOIs are listed in the key resources table.
- Any additional information required to reanalyze the data reported in this paper is available from the lead contact upon request.

EXPERIMENTAL MODEL AND STUDY PARTICIPANT DETAILS

Mice

(1) NCG mice, 6 weeks of age when purchased and approximately 8 weeks of age at study initiation, equal distribution of male and female animals.

Cell lines

(1) IMR-32 (neuroblast cells isolated from 13-month-old Caucasian male).
(2) NLF (NBL line isolated from 3-year-old male).
(3) LAN-1 (NBL cell line isolated from 2-year-old male).
(4) SMS-SAN (NBL cell line isolated from 3-year-old female).
(5) SK-N-AS (neuroblast cells isolated from the brain of a 6-year-old Caucasian female).
(6) SK-N-Be2 (NBL cell line from bone marrow biopsy taken from 2-year-old male).
(7) SH-SY5Y (Subclone of the SK-N-SH cell line, which was established from a metastatic bone tumor of a 4-year-old female).
(8) NCI-H441 (Derived from pericardial fluid of male with papillary adenocarcinoma of the lung).
(9) NCI-H69 (lung carcinoma from 55-year-old Caucasian male).
(10) NCI-526 (isolated from lung of 55-year-old Caucasian male with carcinoma).
(11) A549 (lung carcinoma from 58-year-old Caucasian male).

Cell lines and culture conditions

Human NBL cell lines (IMR-32, NLF, LAN-1, SMS-SAN, SK-N-AS, and SK-N-Be2) were acquired from ATCC and cultured in Advanced RPMI medium (Gibco) supplemented with 10% FBS (Gibco), 1% GlutaMAX (Gibco), and 1% Penicillin/Streptomycin. Human SCLC cell line models (NCI-H441, NCI-H69, and NCI-H526) were cultured in RPMI 1640 (Gibco) supplemented with 10% FBS (Gibco) and 1% Pen/Strep (Gibco). The human lung cancer cell line A549 was cultured in F-12K (Gibco) supplemented with 10% FBS (Gibco) and 1% Pen/Strep (Gibco). Cell cultures were incubated at 37°C with 5% CO_2.

Please cite this article in press as: Stokes et al., Subtype-selective prenylated isoflavonoids disrupt regulatory drivers of MYCN-amplified cancers, Cell Chemical Biology (2023), https://doi.org/10.1016/j.chembiol.2023.11.007

In vivo studies

Forty 6-week old NCG mice were purchased from Charles River Laboratories, comprised equal population of male and female mice, and allowed to acclimate to Columbia's animal barrier facility for one week. SK-N-Be2 cells were suspended at a density of 100×10^6 cells/mL in a 50% matrigel slurry in PBS. 100 μL of this suspension was injected into the right flank, to generate a tumor-forming mass. Tumor volume was monitored at first by palpation and then daily by caliper. As tumors reached approximately 100 mm^3 in volume, mice were randomly assigned to one of four treatment arms: No Treatment (6 mice), Vehicle-Only (8 mice), Isopomiferin at 20 mg/kg (12 mice), or Pomiferin at 20 mg/kg (12 mice). Isopomiferin and pomiferin were dissolved initially into DMSO, then diluted into a solution of 50% w/v 2-hydroxypropyl beta cyclodextrin in 50% ethanol in PBS, to create a 5 mg/mL stock solution. This solution was diluted with PBS to create the appropriate concentration for 20 mg/kg following a 300 μL i.p. injection and filtered through a 0.22 μm syringe filter. The solvent-only control treatment comprised an equivalent solution absent the test compounds. Treatments were administered by i.p. injection once daily in the morning. Tumor volume was measured by caliper and mouse body weight measured using a microscale every-other day. On day 14 of the treatment regimen, two mice from the solvent-only, pomiferin, and isopomiferin treatment groups were euthanized 3 h after treatment and sampled for analysis of MYCN abundance in tumors. Upon completion of the study, mice were euthanized by CO_2 asphyxiation for a minimum of 3 min. All animal experiments were approved by the Columbia University Institutional Animal Care and Use Committee.

METHODS DETAILS

Chemical screening and cell viability assays

For chemical screening, cells were seeded into white opaque 384-well plates at a density of 1000 cells/well and incubated overnight. The following day, 384-well stock screening plates containing 10 mM compound dissolved in dimethyl sulfoxide (DMSO) were diluted to a concentration of 200 μM in daughter plates containing growth medium. From these plates, compounds were diluted 1/10 into the assay plates containing cells, resulting in a final chemical concentration of 20 μM and a DMSO concentration of 0.2%. Cells were incubated for 72 h, after which cell viability was determined using CellTiterGlo luminescence assay, following the manufacturer's instructions (Promega). Compounds were screened from 3 chemical libraries: 727 compounds from the NIH Clinical Collection (National Institutes of Health), 2498 compounds from the NCI Diversity Set (National Cancer Institute) and 2400 compounds from the SPECTRUM Collection (MicroSource). Following the initial screen, lethal molecules were rescreened across a five point, 3-fold dose series ranging from 20 μM to 0.25 μM, following a similar protocol. Dose curves of cell viability were generated using PRISM v7.0 software (GraphPad).

Protein detection by Western blot

Cells were seeded in 6w plates at 400k cells/well and incubated overnight. The following day, compounds were diluted from 10 mM DMSO stocks into growth media to achieve desired concentrations, with DMSO added to control wells to maintain equal concentration across groups. Following treatment, the media was removed and cells were rinsed with cold PBS, followed by trypsin digestion to release cells from the wells. Cells were collected with media and pelleted by centrifugation. Cell pellets were incubated on ice in RIPA lysis buffer, followed by centrifugation at 17 000 × g for 10′ to remove cellular debris. Protein was denatured by boiling in 1X laemmli buffer and separated by gel electrophoresis using NuPAGE 4–12% Bis-Tris protein gels (Thermo Fisher Scientific). Semi-dry protein transfer to nitrocellulose membrane was performed using iBlot 2 dry transfer system (Thermo Fisher Scientific), following manufacturer's instructions. Membranes were blocked by incubating membrane in LI-COR Odyssey blocking buffer (LI-COR Biosciences), at room temperature (RT) for 1 h. Membranes were incubated in primary antibody at 4°C overnight a 1:1000 dilutions. All antibodies were purchased from Cell Signaling Technologies. Following incubation with primary antibody, membranes were washed 3× in PBST, and incubated with secondary antibody (LI-COR Biosystems) for 1 h in Odyssey buffer with 0.2% tween 20. Imaging of membrane luminescence was performed using the Odyssey Western Breeze detection system (LI-COR Biosystems).

RT-qPCR

Total RNA was isolated from cell pellets using the RNeasy RNA isolation kit (QIAGEN), following manufacturer's instructions. RNA abundance and purity was determined using a nanodrop spectrophotometer (Thermo Fisher Scientific). Two μg of total RNA was used as a template to generate cDNA using both oligo-dT and random priming hexameters. cDNA was treated with RNAse A to remove residual RNA, and then diluted 10-fold for qPCR reactions using SYBR green (Invitrogen) and gene-specific qPCR primers (Table S1). qPCR reactions were performed using the Viia7 Real-Time PCR system (Applied Biosystems), and relative transcript abundance evaluated using the deltaCT method, using the GAPDH housekeeping gene as normalization control.

PLATESeq cell culture, library prep, sequencing and analysis

SK-N-Be2 cells were seeded in a 96 well plate at a density of 10 000 cells/well and incubated overnight. The following day, compounds were sequentially diluted from DMSO stock solutions to create desired concentrations, with DMSO at 0.1%. Duplicate plates were created by randomizing 90 lethal molecules across the plate, with the inclusion of six DMSO-only control wells. Following the addition of compounds, the plates were incubated for 24 h. Following treatment, wells were rinsed twice with cold PBS, and 40 μL of Buffer TCL was added to the each well and frozen at −20°C. Library prep and sequencing were performed at Columbia's high-throughput screening core and the JP Sulzberger Genome center, following published protocols.[11]

Please cite this article in press as: Stokes et al., Subtype-selective prenylated isoflavonoids disrupt regulatory drivers of MYCN-amplified cancers, Cell Chemical Biology (2023), https://doi.org/10.1016/j.chembiol.2023.11.007

Reads were mapped against the human reference genome version Grch38 using the STAR aligner and used the variance stabilizing transformation from the DESeq2 package for R to normalize each plate. Next, we corrected for batch effect due to having compounds replicates on separate plates. We used the function *combat* from the sva package for R to compute the batch-corrected normalized gene expression and fitted a linear model for each compound against the set of DMSO controls on each plate (6 wells per plate per DMSO-treated cells). We used the *limma* package for R to fit the linear model and to compute p values and moderated t-statistics for each gene. For each compound, we used a vector of these statistics to generate a gene expression profile of z-scores representing the compound effect as differential between post- and pre-treatment.

We analyzed each compound gene expression profile using the VIPER algorithm[13] with TARGET and NRC NBL interactomes, reverse-engineered and provided in.[8] Specifically, the ARACNe-AP algorithm[33] was used to generate TARGET- and NRC-specific interactomes from cohort-specific NBL gene expression profiles. The TARGET and NRC interactomes comprises 205,271 and 359,846 transcriptional interactions.

VIPER analysis resulted in two protein activity profiles for each compound that were integrated using Stouffer's Z score method.[66] We ran the VIPER algorithm after having pruned each interactome by keeping for each protein regulon the top 100 targets with the highest likelihood, and excluding protein regulons with less than 50 targets, since fixing the number of targets makes more comparable the activity score of each protein within the same profile.

Virtual-Inference of Kinase INhibiton by Gene regulatory networks algorithm

The VIKING algorithm consists in the following steps: 1) Inference of protein activity profiles of individual samples across conditions with VIPER,[13] 2) Generation of high confidence PPI network with PrePPI, 3) PPI Network perturbation analysis with DeMAND,[35] 4) Filtering of top dysregulated kinases with negative NES as inferred by VIPER between post- and pre-treatment conditions (Figure S5).

We used ARACNe[33] to reverse-engineer a regulatory network based on recent RNA-Seq data of 157 tumors from NBL patients collected by the TARGET consortium. The resulting network consists of 2,362 TFs and co-TFs, and 3,197 signaling molecules, yielding a total of 5,559 regulatory proteins, 21,664 targets and 1,889,970 interactions. This interactome was used to compute a sample-specific protein activity signature with the VIPER algorithm, for 6 isopomiferin-treated samples and 6 samples treated with pomiferin null analog (pomiferin dimethyl ether), all collected at 24 h. For this analysis, each regulon was pruned as described above.

We generated a PPI network from the PrePPI database[36] by selecting for pairs of protein interactions having structural score above the median of the data for the specific PPI. The PPI list was further refined by filtering out interactions of proteins not known to have regulatory functions, keeping therefore TF, co-TF, and signaling proteins. The network was then expanded by collecting for each protein its top scoring interactions and applying the same aforementioned criteria. This process was iterated 5 times, allowing the construction of a neighborhood of high-confidence PPI for each regulatory protein. This procedure yielded to a PPI network of 201,193 high-confidence interactions. Next, the DeMAND algorithm was used to prioritize a list of 5,559 proteins based on the inferred dysregulation of a protein and all its predicted interaction partners between the set of treatment samples and the controls. The resulting list of MoA proteins was filtered accordingly several criteria, including a Bonferroni corrected p value lesser than 0.01 for DeMAND scores, NES score lesser than -1.965 for VIPER scores, and filtering out proteins that are not kinases. We used annotation for 514 human kinases as described in,[67] and retained all regulatory proteins contained in this set.

The VIKING algorithm requires genome-wide drug perturbation RNASeq profiles in a number of samples per replicate ≥ 6 (see DeMAND algorithm requirements). Given that these data are generally not available, CRISPR KO and RNAi screening data were used, as released by the Broad Institute through the Cancer Dependency Map (DepMap) Consortium, downloaded respectively in May 2023 and January 2021. From these data, the NBL MYCNA SK-N-Be2 line was selected to make data comparable with our drug screening performed on the same line. The ROC curve was built using VIKING predictions on isopomiferin drug perturbations over SKNBE2 cells (n = 12 treatments and n = 6 controls) and compared against gene dependency scores on SKNBE2 cells, integrated across the two platforms (i.e., CRISPR and RNAi) to control for technology bias. Top 5% of gene dependency scores were considered as the genes whose KO/interference affect cell viability. The Area Under the Curve (AUROC) computed with this approach is 70.8%, with $\sim$50% sensitivity at $\sim$95% specificity (Figure S5E).

Quantification of cellular accumulation of compounds

Cellular accumulation of CX-4945 and pomiferin was quantified by LC-MS following previously published protocols.[68,69] In brief, SK-N-Be2 cells were seeded at 400k cells/well in 6 w plates and incubated overnight. The following day, compounds were added to wells at indicated concentrations, with DMSO-only control added to non-treated wells. Following treatment for the indicated time periods, cells were trypsinized, rinsed twice with cold PBS to remove media, pelleted by centrifugation, and frozen at -20°C. To extract compounds, frozen pellets were resuspended in 150 μL of acetonitrile, sonicated for 2′, and centrifuged at 1400 x g for 75′ at 4°C. Supernatant was collected and analyzed by LC-MS using a system comprised a Thermo Scientific Dionex Ultimate 3000 and a Bruker amaZon SL equipped with an electrospray ionization source controlled by a Bruker Hystar 3.2. Compounds were separated by injecting 20 μL of supernatant onto an Agilent Eclipse Plus C18 column (2.1 × 50 mm, 3.5 μM) maintained at 20°C, with the flow rate set at 400 μL/min. Initial flow conditions were 60% solvent A (MilliQ H_20, 0.1% acetic acid), and 40% solvent B (HPLC-grade MeOH, 0.1% acetic acid). Solvent B was raised to 60% over 0.25 min and to 70% by 6.75 min. Solvent B was raised to 95% by 7 min and lowered back to 40% by 8 min; total run time was 9 min.[70]

Please cite this article in press as: Stokes et al., Subtype-selective prenylated isoflavonoids disrupt regulatory drivers of MYCN-amplified cancers, Cell Chemical Biology (2023), https://doi.org/10.1016/j.chembiol.2023.11.007

Biochemical kinase assays

Cell-free biochemical kinase assays were performed at Reaction Biology Corporation (Malvern, PA). In brief, kinase substrates were diluted into reaction buffer containing 20 mM HEPES (pH 7.5), 10 mM $MgCl_2$, 1 mM EGTA, 0.02% Brij35, 0.02 mg/mL BSA, 0.1 mM Na_3VO_4, 2 mM DTT, 1% DMSO. Purified protein (CK2a1, CK2a2, or mTOR) was added to the substrate solution and gently mixed. Test compounds were diluted from 10 mM DMSO stock solutions into the reaction buffer using an Echo550 acoustic dispenser, followed by incubation at RT for 20 min 33P-ATP (10 μCi/μL) was added to reaction mixture, following incubation for 2 h at RT. Reactions were then spotted onto P81 ion exchange paper and kinase activity was detected by filter binding method.

In vitro metabolic stability assays

Mouse liver microsomes (Xenotech) were diluted to 0.5 mg/mL in a solution containing 100 mM PBS buffer at 7.4 pH, an NADPH regenerating system (Promega), and test compounds at 20 μM. The mixture was incubated at 37°C under gentle rotation for the indicated time points. The reaction was quenched by aliquoting 15 μL of solution into 60 μL ice-cold acetonitrile containing an internal standard. Test compounds were quantified by LC-MS using a system comprised a Thermo Scientific Dionex Ultimate 3000 and a Bruker amaZon SL equipped with an electrospray ionization source controlled by a Bruker Hystar 3.2. Compounds were separated by injecting 20 μL of sample onto an Agilent Eclipse Plus C18 column (2.1 × 50 mm, 3.5 μM) maintained at 20°C, with the flow rate set at 400 μL/min. Initial flow conditions were 60% solvent A (MilliQ H_20, 0.1% acetic acid), and 40% solvent B (HPLC-grade MeOH, 0.1% acetic acid). Solvent B was raised to 60% over 0.25 min and to 70% by 6.75 min. Solvent B was raised to 95% by 7 min and lowered back to 40% by 8 min; total run time was 9 min.

Mouse plasma was diluted with 100 mM PBS buffer at 7.4 pH at a 1:1 ratio and warmed to 37°C. Test compounds were added to the plasma solution at 20 μM and incubated for the indicated time point. Reactions was quenched by aliquoting 15 μL of solution into 60 μL ice-cold acetonitrile containing an internal standard. Compounds were quantified by LC-MS, as described above.

Protein expression

Recombinant HIS-tagged CK2a1 protein was expressed in BL21 *Escherichia coli* from a codon-optimized expression system driven by an IPTG-inducible promoter. Bacteria were selected from a single successful transformation on selectable agar plates and cultured in 2-YT broth with 100 μg/mL ampicillin at 37°C until the culture reached an OD600 of 0.8. The culture was then acclimated to 20°C for 1 h, following which IPTG was added at 0.5 mM and the culture was incubated overnight at 20°C. The following day, the culture was pelleted at 4000 rpm for 20 min at 4°C. The pellet was resuspended in buffer (50 mM Tris-Cl pH 8.0, 500 mM NaCl, and protease inhibitor tablets) and lysed by sonication. Bacterial lysate was centrifuged at 14000 rpm for 35 min at 4°C, and the supernatant was incubated with Ni Sepharose 6 Fast Flow beads that were equilibrated in buffer (50 mM Tris-Cl pH 8.0, 500 mM NaCl). Affinity purification using was performed following manufacturer's instructions (GE Healthcare). Eluted protein was dialyzed overnight at 4°C in buffer (50 mM Tris-Cl and 300 mM NaCl) to remove imidazole. The following day, dialyzed protein was concentrated by centrifugation through amicon ultracell 10 kDa cutoff filter columns (EMD Millipore), followed by FPLC protein purification. Protein abundance was quantified by Bradford protein assay (BioRAD) and purity evaluated by Coomassie staining of SDS-PAGE gels and Western blot.

Molecular modeling studies

Molecular docking, molecular modeling, and visualizations were performed using Glide (version 2020-4, Schrödinger) and Schrödinger Maestro (version 2020-4). Pomiferin was docked in a crystal structure of CK2 (PDB ID: 3Q9W).

Semi-synthesis of pomiferin and osajin analogs

Pomiferin and osajin were isolated from *Maclura pomifera* by Soxhlet extraction of the dried fruit with hexane and ether to give a 1:1 mixture of the two. RP HPLC separated pomiferin and osajin and small amounts of structurally related isoflavones. Treatment of the mixture of pomiferin and osajin with iodomethane and potassium carbonate in acetone gave the di-*O*-methyl (AZVII-89-11) and mono-*O*-methyl (AZVII-89-12) derivatives, respectively. By treatment of pomiferin with iodomethane and potassium carbonate in acetone the O-methyl analog (AZVII-4A) could be isolated. Catalytic hydrogenation of the pomiferin/osajin mixture gave the respective hydrogenated derivatives (AZVII-12P and AZVII-12O, respectively) after purification by RP HPLC as well as minor amounts of reduced structurally related isoflavones (AZVII-12-1 and AZVII-12-2).

Extraction of prenylated isoflavonoids from osage orange

Osage oranges (*Maclura pomifera*) were collected, chopped up, oven dried at 80°C, and pulverized in a corn meal grinder. The resulting powder was placed in a Soxhlet extractor and extracted with hexane, followed by ether. The ether extracts were concentrated to give an orange crystalline solid containing approximately a 1:1 mixture of pomiferin and osajin, as determined by 1H NMR. Reversed phase HPLC separation (CH3CN/H20/0.01%TFA, 60–90% CH3CN, 15-min gradient) of 100 mg of the mixture gave two major and three minor peaks corresponding to pomiferin (44.6 mg yellow powder, RT = 14.1 min), osajin (36.2 mg pale yellow powder, RT = 17.1 min), AZVII-13-1 (RT = 7.2 min), AZVII13-2 (RT = 9.9 min), and AZVII13-3 (RT = 12.3 min), respectively.

Please cite this article in press as: Stokes et al., Subtype-selective prenylated isoflavonoids disrupt regulatory drivers of MYCN-amplified cancers, Cell Chemical Biology (2023), https://doi.org/10.1016/j.chembiol.2023.11.007

AZVII-13-1 (5,7-dihydroxy-3-(4-hydroxyphenyl)-6-(3-methylbut-2-en-1-yl)-4*H*-chromen-4-one)

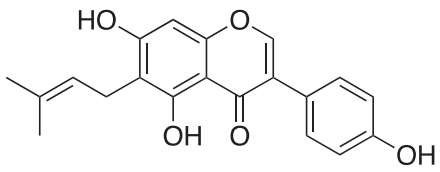

1H NMR (CD3OD) δ 8.03 (s, 1H), 7.37 (d, J = 8.6 Hz, 2H), 6.85 (d, J = 8.6 Hz, 2H), 6.38 (s, 1H), 5.21–5.27 (m, 1H), 1.78 (s, 3H), 1.66 (s, 3H). MS M + H = 339.1.

AZVII-13-2 (diprenylorobol; 3-(3,4-dihydroxyphenyl)-5,7-dihydroxy-6,8-bis(3-methylbut-2-en-1-yl)-4*H*-chromen-4-one)

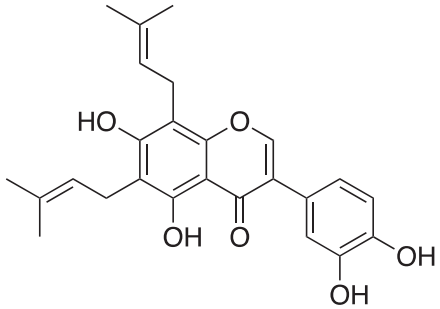

1H NMR (CD3OD) δ 8.10 (s, 1H), 7.03 (d, J = 1.9 Hz, 1H), 6.86 (dd, J = 1.9, 8.2 Hz, 1H), 6.82 (d, J = 8.2 Hz, 1H), 5.28–5.12 (m, 2H), 3.49 (d, J = 7.0 Hz, 2H), 3.39 (d, J = 7.1 Hz, 2H), 1.82 (s, 3H), 1.80 (s, 3H), 1.68 (s, 6H). MS M + H = 422.2.

AZVII-13-3 (diprenylgenistein; 5,7-dihydroxy-3-(4-hydroxyphenyl)-6,8-bis(3-methylbut-2-en-1-yl)-4*H*-chromen-4-one)

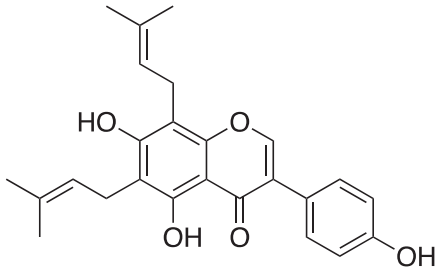

1H NMR (CD3OD) δ 8.12 (s, 1H), 7.38 (d, J = 8.6 Hz, 2H), 6.85 (d, J = 8.6 Hz, 2H), 5.24–5.15 (m, 2H), 3.49 (d, J = 7.4 Hz, 2H), 3.39 (d, J = 7.1 Hz, 2H), 1.82 (s, 3H), 1.80 (s, 3H), 1.68 (s, 6H). MS M + H = 407.2.

Hydrogenation of pomiferin and isopomiferin

An approximately 1:1 pomiferin:osajin mixture (164 mg) in methanol (15 mL) was treated with 10% Pd/C (30 mg) and hydrogen gas (balloon pressure) at RT. After 18 h the mixture was filtered through Celite and concentrated in vacuum to give a colorless solid. Separation by RP HPLC (CH_3CN/H_20/0.01%TFA, 60–90% CH_3CN, 15-min gradient) gave two major and two minor peaks corresponding to AZVII-12P (RT = 14.1 min), AZVII-12O (RT = 16.9 min), AZVII-12-1 (RT = 10.8 min), and AZVII-12-2 (RT = 13.2 min), respectively.

Please cite this article in press as: Stokes et al., Subtype-selective prenylated isoflavonoids disrupt regulatory drivers of MYCN-amplified cancers, Cell Chemical Biology (2023), https://doi.org/10.1016/j.chembiol.2023.11.007

AZVII-12P (3-(3,4-dihydroxyphenyl)-5-hydroxy-6-isopentyl-8,8-dimethyl-2,3,9,10-tetrahydro-4*H*,8*H*-pyrano[2,3-*f*]chromen-4-one)

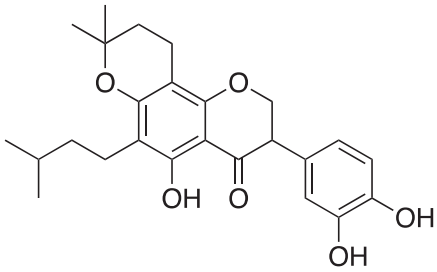

1H NMR (CD3OD) δ 6.75 (d, J = 8.2 Hz, 1H), 6.71 (d, J = 2.1 Hz, 1H), 6.62 (dd, J = 8.2,2.1 Hz, 1H), 4.58 (dd, J = 7.2, 11.3 Hz, 1H), 4.52 (dd, J = 5.0, 11.3 Hz, 1H), 3.79 (dd, J = 7.2, 5.0 Hz, 1H), 2.61 (t, J = 6.9 Hz, 2H), 2.52 (t, J = 6.9 Hz, 2H), 1.80 (t, J = 6.9 Hz, 2H), 1.53 (sept, J = 6.6 Hz, 1H), 1.36 (s, 3H), 1.35 (s, 3H), 0.94 (d, J = 6.6 Hz, 6H) MS M + H = 424.2.

AZVII-12O (5-hydroxy-3-(4-hydroxyphenyl)-6-isopentyl-8,8-dimethyl-2,3,9,10-tetrahydro-4*H*,8*H*-pyrano[2,3-*f*]chromen-4-one)

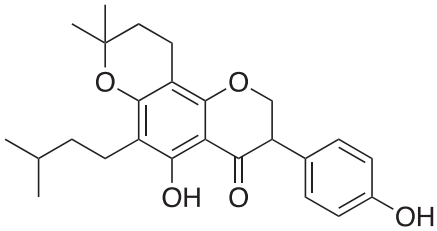

1H NMR (CD3OD) δ 7.10 (d, J = 8.6 Hz, 2H), 6.76 (d, J = 8.6 Hz, 2H), 4.58 (dd, J = 5.3, 11.3 Hz, 1H), 4.53 (dd, J = 7.9, 11.3 Hz, 1H), 3.89 (dd, J = 5.3, 7.9 Hz, 1H), 2.61 (t, J = 6.9 Hz, 2H), 2.52 (t, J = 6.9 Hz, 2H), 1.80 (t, J = 6.9 Hz, 2H), 1.52 (sept, J = 6.6 Hz, 1H), 1.36 (s, 3H), 1.35 (s, 3H), 0.93 (d, J = 6.6 Hz, 6H) MS M + H = 408.2.

AZVII-12-1 (3-(3,4-dihydroxyphenyl)-5,7-dihydroxy-6,8-diisopentylchroman-4-one)

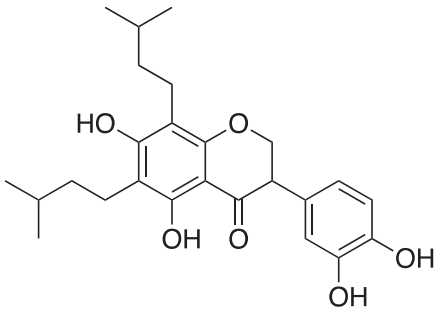

1H NMR (CD3OD) δ 6.73 (d, J = 8.2 Hz, 1H), 6.71 (d, J = 2.2 Hz, 1H), 6.62 (dd, J = 2.2, 8.2 Hz, 1H), 4.53 (dd, J = 4.8, 11.3 Hz, 1H), 4.47 (dd, J = 7.1, 11.3 Hz, 1H), 3.76 (dd, J = 4.8, 7.1 Hz, 1H), 2.62–2.54 (m, 4H), 1.64–1.47 (m, 2H), 1.40–1.29 (m, 4H), 0.95 (d, J = 5.3 Hz, 6H), 0.93 (d, J = 5.3 Hz, 6H). MS M + H = 428.2.

Please cite this article in press as: Stokes et al., Subtype-selective prenylated isoflavonoids disrupt regulatory drivers of MYCN-amplified cancers, Cell Chemical Biology (2023), https://doi.org/10.1016/j.chembiol.2023.11.007

AZVII-12-2 (5,7-dihydroxy-3-(4-hydroxyphenyl)-6,8-diisopentylchroman-4-one)

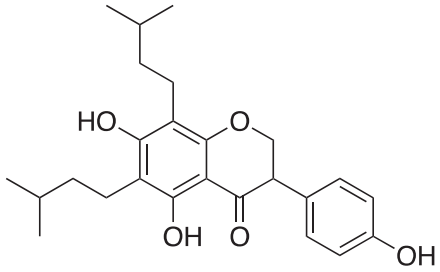

1H NMR (CD3OD) δ 7.11 (d, J = 8.6 Hz, 2H), 6.75 (d, J = 18.6 Hz, 2H), 4.54 (dd, J = 5.0, 11.3 Hz, 1H), 4.48 (dd, J = 7.5, 11.3 Hz, 1H), 3.84 (dd, J = 5.0, 7.5 Hz, 1H), 2.53–2.63 (m, 4H), 1.65–1.48 (m, 2H), 1.42–1.24 (m, 4H), 0.95 (d, J = 4.5 Hz, 6H), 0.93 (d, J = 4.4 Hz, 6H). MS M + H = 412.2.

Methylation of pomiferin and osajin mixture

To an approximately 1:1 mixture of pomiferin:osajin (50 mg) in acetone (2 mL) was added K2CO3 (84 mg) and CH3I (15 μL). After 1 h an additional 30 μL of CH3I was added. After 48 h the reaction mixture was filtered, concentrated and purified by RP HPLC to give 5-hydroxy-3-(4-methoxyphenyl)-8,8-dimethyl-6-(3-methylbut-2-en-1-yl)-4*H*,8*H*-pyrano[2,3-*f*]chromen-4-one and 3-(3,4-dimethoxyphenyl)-5-hydroxy-8,8-dimethyl-6-(3-methylbut-2-en-1-yl)-4*H*,8*H*-pyrano[2,3-*f*]chromen-4-one.

AZVII-89-11 3-(3,4-dimethoxyphenyl)-5-hydroxy-8,8-dimethyl-6-(3-methylbut-2-en-1-yl)-4*H*,8*H*-pyrano[2,3-*f*]chromen-4-one

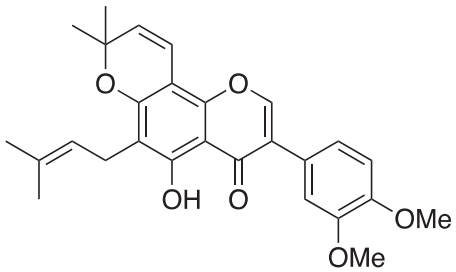

1H NMR (DMSO-d6) δ 13.40 (s, 1H), 8.49 (s, 1H), 7.17 (d, J = 2.1 Hz, 1H), 7.14 (dd, J = 8.3, 2.1 Hz, 2H), 7.03 (d, J = 8.3 Hz, 1H), 6.69 (d, J = 10.0 Hz, 1H), 5.80 (d, J = 10.0 Hz, 1H), 5.22–5.08 (m, 1H), 3.79 (s, 3H), 3.78 (s, 3H), 3.25 (d, J = 7.4 Hz, 2H), 1.75 (s, 3H), 1.63 (s, 3H), 1.44 (s, 6H). MS M + H = 448.2.

AZVI-89-12 5-hydroxy-3-(4-methoxyphenyl)-8,8-dimethyl-6-(3-methylbut-2-en-1-yl)-4*H*,8*H*-pyrano[2,3-*f*]chromen-4-one

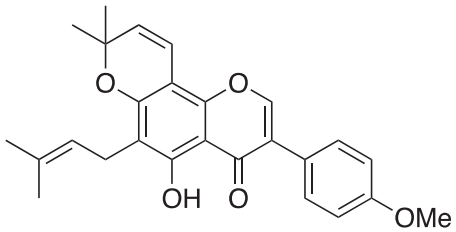

1H NMR (DMSO-d6) δ 13.38 (s, 1H), 8.46 (s, 1H), 7.51 (d, J = 8.8 Hz, 2H), 7.01 (d, J = 8.8 Hz, 2H), 6.69 (d, J = 10.0 Hz, 1H), 5.80 (d, J = 10.0 Hz, 1H), 5.31–4.89 (m, 1H), 3.79 (s, 3H), 3.27–3.22 (m, 2H), 1.75 (s, 3H), 1.63 (s, 3H), 1.44 (s, 6H). MS M + H = 418.2.

Methylation of pomiferin

To pomiferin (50 mg) in acetone (2 mL) was added K_2CO_3 (84 mg) and CH_3I (30 μL). After 2 h an additional 30 μL of CH_3I was added. After 48 h the reaction mixture was filtered, concentrated and purified by RP HPLC to give (5-hydroxy-3-(3-hydroxy-4-methoxyphenyl)-8,8-dimethyl-6-(3-methylbut-2-en-1-yl)-4*H*,8*H*-pyrano[2,3-*f*]chromen-4-one).

Please cite this article in press as: Stokes et al., Subtype-selective prenylated isoflavonoids disrupt regulatory drivers of MYCN-amplified cancers, Cell Chemical Biology (2023), https://doi.org/10.1016/j.chembiol.2023.11.007

AZVII-4A (5-hydroxy-3-(3-hydroxy-4-methoxyphenyl)-8,8-dimethyl-6-(3-methylbut-2-en-1-yl)-4*H*,8*H*-pyrano[2,3-*f*]chromen-4-one)

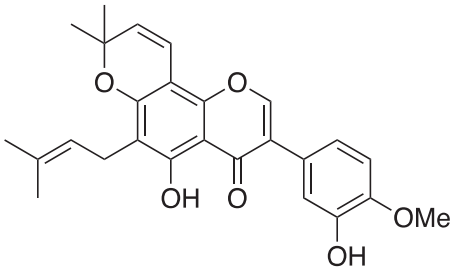

1H NMR (CD3OD) δ 8.14 (s, 1H), 7.06 (bd s, 1H), 6.99 (bd s, 2H), 6.74 (d, J = 9.8 Hz, 1H), 5.69 (d, J = 9.8 Hz, 1H), 5.34–5.08 (m, 1H), 3.89 (s, 3H), 1.80 (s, 3H), 1.80 (s, 3H), 1.67 (s, 3H), 1.47 (s, 6H). MS M + H = 434.2.

Triacetylation of pomiferin

A mixture of pomiferin (100 mg) and NaOAc (600 mg) in acetic anhydride (7.5 mL) was heated in an oil bath at 150°C for 3 h. After cooling to RT, the mixture was poured into water (20 mL) and stored at 4°C overnight. Filtration gave 4-(5-acetoxy-8,8-dimethyl-6-(3-methylbut-2-en-1-yl)-4-oxo-4*H*,8*H*-pyrano[2,3-*f*]chromen-3-yl)-1,2-phenylene diacetate as a gray solid (96 mg).

AZVII-44 4-(5-acetoxy-8,8-dimethyl-6-(3-methylbut-2-en-1-yl)-4-oxo-4*H*,8*H*-pyrano[2,3-*f*]chromen-3-yl)-1,2-phenylene diacetate

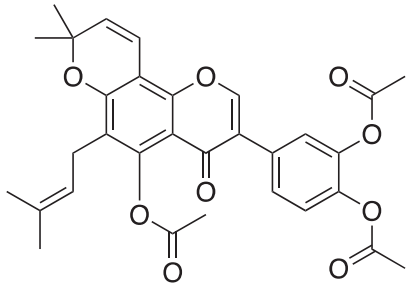

1H NMR (CDCl3) δ 7.85 (s, 1H), 7.41–7.32 (m, 2H), 7.22 (d, J = 8.9 Hz, 1H), 6.76 (d, J = 10.0 Hz, 1H), 5.69 (d, J = 10.0 Hz, 1H), 5.24–4.87 (m, 1H), 2.43 (s, 3H), 2.29 (s, 6H), 1.78 (s, 3H), 1.67 (s, 3H), 1.49 (s, 6H). MS M + H = 546.2.

QUANTIFICATION AND STATISTICAL ANALYSIS

Analysis was performed in R v3.6, and most of the figures were generated using ggplot2.[71] Tabular data were handled with tidyverse.[72] Statistical parameters and tests are reported in the main text, figures, figure legends and tables. Whenever appropriate, p values were adjusted for multiple hypothesis testing using the *p.adjust* function from the stats package in R, using Benjamin-Hochberg method where not otherwise specified. All statistical tests used are described in the relative methods section. Data are considered statistically significant in applied statistical analyses when the p value is less than 0.05, unless explicitly stated that a different significance threshold was employed.